Bioactive Materials 42 (2024) 433–448

Contents lists available at ScienceDirect

Bioactive Materials

journal homepage: www.keaipublishing.com/en/journals/bioactive-materials

Antimicrobial hydrogel foam dressing with controlled release of gallium maltolate for infection control in chronic wounds

Ziyang Lan [a], Leopold Guo [a], Alan Fletcher [a], Nicolai Ang [a], Canaan Whitfield-Cargile [b], Laura Bryan [c], Shannara Welch [d], Lauren Richardson [b], Elizabeth Cosgriff-Hernandez [a,*]

[a] Department of Biomedical Engineering, the University of Texas at Austin, Austin, TX, 78712, USA
[b] Department of Large Animal Medicine, University of Georgia, Athens, GA, 30602, USA
[c] Department of Pathobiology, Texas A&M University, College Station, TX, 77843, USA
[d] Clinical Microbiology Lab, Veterinary Teaching Hospital, Texas A&M University, College Station, TX, 77843, USA

ARTICLE INFO

Keywords:
Chronic wounds
Hydrogel foam
Antimicrobials wound dressing
Infection control
Microsphere

ABSTRACT

Effective treatment of infection in chronic wounds is critical to improve patient outcomes and prevent severe complications, including systemic infections, increased morbidity, and amputations. Current treatments, including antibiotic administration and antimicrobial dressings, are challenged by the increasing prevalence of antibiotic resistance and patients' sensitivity to the delivered agents. Previous studies have demonstrated the potential of a new antimicrobial agent, Gallium maltolate (GaM); however, the high burst release from the GaM-loaded hydrogel gauze required frequent dressing changes. To address this need, we developed a hydrogel foam-based wound dressing with GaM-loaded microspheres for sustained infection control. First, the minimal inhibitory and bactericidal concentrations (MIC and MBC) of GaM against two *Staphylococcus aureus* strains isolated from chronic wounds were identified. No significant adverse effects of GaM on dermal fibroblasts were shown at the MIC, indicating an acceptable selectivity index. For the sustained release of GaM, electrospraying was employed to fabricate microspheres with different release kinetics. Systematic investigation of loading and microsphere size on release kinetics indicated that the larger microsphere size and lower GaM loading resulted in a sustained GaM release profile over the target 5 days. Evaluation of the GaM-loaded hydrogel dressing demonstrated cytocompatibility and antibacterial activities with a zone of inhibition test. An equine distal limb wound model was developed and utilized to demonstrate the efficacy of GaM-loaded hydrogel foam *in vivo*. This antimicrobial hydrogel foam dressing displayed the potential to combat methicillin-resistant *S. aureus* (MRSA) infection with controlled GaM release to improve chronic wound healing.

1. Introduction

Chronic wounds have become a growing healthcare problem worldwide, with increased financial and mental burdens on nearly 50 million patients worldwide [1,2]. One of the challenges in chronic wound healing is a wound infection caused by the colonization of bacteria or other microorganisms [3]. In a chronic wound, the long-term disruption of the skin's physical barrier is accompanied by the denaturation of the local proteins, glycans, and lipids, providing a nutrient-rich environment for bacterial adherence and growth [4]. Bacterial infection arrests the wound healing in the persistent inflammation stage and significantly delays the structural reconstruction and functional restoration of chronic wounds. Furthermore, infection-caused wound deterioration and necrosis may lead to lower extremity amputation or severe chronic wound complications, including systemic sepsis [5,6].

The pathogenesis of bacterial infection and its high complexity must be appreciated before designing and evaluating any infection control measures. The bacteria on a chronic wound bed demonstrate a continuum from contamination through colonization to infection [7].

Peer review under responsibility of KeAi Communications Co., Ltd.
* Corresponding author. 107 W. Dean Keeton BME Building, Room 3D Austin, TX, 78712, USA.
E-mail addresses: ziyangl@utexas.edu (Z. Lan), leopold.guo@utexas.edu (L. Guo), alan.fletcher@utexas.edu (A. Fletcher), nicolai.ang@utexas.edu (N. Ang), wcana@uga.edu (C. Whitfield-Cargile), lbryan@cvm.tamu.edu (L. Bryan), swelch@exchange.tamu.edu (S. Welch), lr22859@uga.edu (L. Richardson), cosgriff.hernandez@utexas.edu (E. Cosgriff-Hernandez).

https://doi.org/10.1016/j.bioactmat.2024.08.044
Received 21 June 2024; Received in revised form 27 August 2024; Accepted 31 August 2024

Researchers have identified the minimal colonization (10^5 organisms/g of tissue) that can impede wound healing [8]. As the higher bacterial colonization density, bacterial proliferation overcomes the host immune responses, resulting in tissue damage and transition to infection. Moreover, bacterial colonization in chronic wounds is polymicrobial, as 76 % of the ulcers presented two or more bacterial species, increasing the difficulty in eliminating all the resident bacteria and infection control [9]. Bacterial adherence and colonization can also lead to biofilm formation that greatly impedes wound healing because the biofilm formation results in extreme difficulty in eradicating bacteria, ulcer enlargement, failure of any wound treatments, and systemic infection of the patient [10,11]. Overall, bacterial infection and biofilm formation induced persistent inflammation in the wound site, causing the overproduction of reactive oxygen species (ROS) and matrix metalloproteases (MMPs) [12,13]. Elevated oxidative stress and proteolytic enzymes of high concentrations hinder cell growth, extracellular matrix reconstruction, and sequential angiogenesis, substantially delaying wound healing. Therefore, a first-line wound dressing with effective infection control is required to achieve accelerated and improved healing of chronic wounds.

Current modalities to mitigate bacterial infection in chronic wounds include applying one or more antimicrobial agents, employing smart biomaterials that stimulate controlled production of ROS and MMPs, and designing biomaterials with customized nano-topography for targeted immunoregulation and anti-fouling activities [14–17]. Among them, applying antimicrobial agents is deemed the most cost-effective and accessible strategy. Commercially available antimicrobial agents include antibiotics, silver-based particles, iodine-containing agents, and antimicrobial peptides. The excessive and unsupervised use of antibiotics has greatly contributed to the growing bacterial resistance to these agents, lowering their efficacy and increasing the wound treatment cost [18,19]. Several bacterial strains afflicting diabetic foot ulcers have been found resistant to commonly applied antibiotics, such as penicillin and cephalosporins [20]. Wound dressings containing iodine and silver have been administered topically to avoid negative systemic effects, effectively controlling bacterial infection and preventing biofilm formation. However, iodine-loaded dressings cannot be used on patients with thyroid disorders and patients who are pregnant or lactating due to systemic absorption [21,22]. Silver is limited by potential bacterial resistance development and negative effects on patients, such as local cytotoxicity and allergic responses. Chlorhexidine and polyhexamethylene biguanide (PHMB) are also loaded in antimicrobial dressings for chronic wound treatment. Nonetheless, exposure-based chlorhexidine allergies and slight systemic toxicity by PHMB place health risks on the patients [23–28]. In addition, natural and synthetic antimicrobial peptides display antimicrobial efficacy. Still, their employment is confined by manufacturing and storage costs, loss of bioactivity, susceptibility to peptidase, and potential cytotoxicity [29]. Herein, we investigated a new antimicrobial agent, gallium maltolate (GaM), to combat chronic wound infection as it shows less chance for bacterial resistance development, facilitates both topical and systemic medications, and potentially promotes wound healing. GaM has high solubility in both water and lipids that facilitate its transportation in different media and interfere with iron-dependent metabolic activities, such as gene expression and DNA replication [30].

A previous study has reported a 3D-printed hydrogel gauze loaded with GaM that demonstrated bactericidal activity against *Staphylococcus aureus (S. aureus)*, including methicillin-resistant *S. aureus* (MRSA) [31]. This GaM-loaded gauze reduced the wound bacterial load in a murine splinted-wound model without showing adverse effect on wound closure. However, over 95 % of the loaded GaM was released in the first 6 h after dressing application, thus requiring a frequent dressing change to prevent bacteria regrowth. A delivery system is needed to achieve more sustained GaM release for prolonged infection control. Poly (lactic-co-glycolic) acid (PLGA) microspheres have been widely used to design drug delivery systems due to their biocompatibility and tunable biodegradability [32–34]. There are currently more than twenty different types of PLGA-based microspheres approved for use in the market [35]. Different fabrication methods of PLGA microspheres include emulsification, microfluidic technology, electrospraying, and spray drying. Comparatively, electrospraying has demonstrated high tunability of microsphere size and morphology, allowing for one-step preparation with high yield and reproducibility [36]. Control of microsphere composition and the electrospraying parameters (voltage, collection distance, and solution viscosity) allows for the modulation of GaM loading and microsphere size that we hypothesize will enable different GaM release profiles. A target release profile would provide a burst GaM release to eliminate existing bacteria and a sustained release above the therapeutic concentration for long-term inhibition of bacterial growth.

In this paper, we describe the development antimicrobial hydrogel foam dressing encapsulating GaM-loaded PLGA microspheres to achieve a controlled release of GaM. The antimicrobial activities of GaM against wound-specific *S. aureus* strains (MSSA 29213 and MRSA 43300) were investigated with an improved microdilution assay. The effects of GaM on dermal fibroblasts were studied. GaM-loaded PLGA microspheres with varied microsphere sizes and GaM loading were prepared by adjusting the electrospraying conditions. GaM-loaded microspheres were then encapsulated in a previously reported porous hydrogel foam dressing to impart self-tuning moisture maintenance and infection control [37]. Antimicrobial hydrogel foams were tested in a custom transmembrane release model to characterize the GaM release profiles, cytocompatibility, and bactericidal activity. Finally, the *in vivo* efficacy of this antimicrobial hydrogel foam was assessed using an infected equine distal limb wound model that simulated the healing mechanism and nutrient-deficiency condition of human chronic wounds. Altogether, this work aimed to elucidate the effects of GaM on wound-related bacteria and cells and evaluate the efficacy of GaM-loaded antimicrobial hydrogel foam in infection control.

2. Materials and methods

2.1. Materials

All chemicals were purchased from Sigma Aldrich (Milwaukee, WI) and used as received unless otherwise noted.

2.2. Antibacterial activity

2.2.1. Bacterial culture

A single colony of methicillin-susceptible *Staphylococcus aureus* (MSSA, 29213; ATCC®, Manassas, VA) commonly found in wound infection was isolated and cultured in Brain Heart Infusion broth (BHIB) and incubated at 37 °C for 16–18 h. RPMI 1640 medium (Caisson Labs Inc., Smithfield, UT) was supplemented with 2 mM GlutaMAX™ (Thermo Fisher Scientific, Waltham, MA) and 1 mM sodium pyruvate (Thermo Fisher Scientific). After centrifugation at 3000*g* for 10 min, the bacterial cells formed the pellet and were then resuspended in RPMI. As described previously, a standard curve was established between colony-forming units per volume and the optical density ($\lambda = 625$ m) of the bacterial inoculum to determine the bacterial density in RPMI [38]. Likewise, a bacterial inoculum in RPMI was prepared with wound-associated methicillin-resistant *Staphylococcus aureus* (MSSA, 43300; ATCC®, Manassas, VA).

2.2.2. Determination of MIC and MBC

The antibacterial effect of GaM (Gallixa LLC, Menlo Park, CA) was studied by the minimal inhibitory concentration (MIC) and minimal bactericidal concentration (MBC) using a microdilution assay according to the CLSI guidelines [39]. GaM stock in supplemented RPMI was constituted at 16,000 μM, sterile filtered, and diluted to designated concentrations. The bacteria inoculum (MSSA 29213 or MRSA 43300)

was added to each concentration (n = 3) to obtain a two-fold dilution and yield final GaM concentrations ranging from 250 to 8000 μM in a 96-well plate. The initial bacterial density was 5×10^5 colony-forming units (CFU)/ml. Sterile RPMI and untreated MSRA were used as positive and negative controls, respectively. The plate was then incubated at 37 °C for 24 h at 45 rpm. The optical density of the bacterial inoculum was measured spectrophotometrically at 625 nm before and after treatment, and bacterial density was determined by counting the colony units after a serial 10-fold dilution in BHIB after 24-h culture. MIC was determined as the lowest concentration that inhibits bacterial growth when the treated bacterial density (in CFU/ml) showed no statistically significant difference from the initial bacterial density. Also, the MBC of GaM was evaluated quantitatively and was defined as the concentration at which the treated bacterial density was lower than 0.1 % of the initial bacterial density. The same method was applied to determine the MIC and MBC of gentamicin sulfate and vancomycin hydrochloride against MSSA 29213 and MRSA 43300. All the studies were triplicated for statistical analysis.

2.3. Cell viability and selectivity index

The cellular effects of GaM and gentamicin sulfate were studied on human dermal fibroblasts (hDFs). The antimicrobial agent's half-maximal inhibitory concentration (IC_{50}) on different cell lines was identified and utilized to calculate the selectivity index (IC_{50}/MIC) with a cell viability assay. For the cell viability study, hDFs were cultured in 48-well plates at an initial density of 30,000 cells/well and incubated at 37 °C for 24 h. Culture media was then replaced by pre-constituted treatments with the antimicrobial agent at concentrations ranging from 25 to 15,000 μM (n = 3/concentration). Cells grown on tissue culture polystyrene and treated with 70 % ethanol served as positive and negative controls, respectively. After the treatment, resazurin was diluted in the culture media under the manufacturer's instruction and replaced the treatments, followed by a 4-h incubation at 37 °C. For treatments and controls, the fluorescence intensity was measured spectrophotometrically (ex: 544 nm/em: 590 nm). The relative cell viability was calculated by normalizing the treatment readout to the positive control ones. The IC_{50} was then derived with an embedded algorithm in GraphPad Prism, "dose-response inhibition". The mean values of IC_{50} were then used to calculate the selectivity indices (IC_{50}/MIC) of GaM, gentamicin, and vancomycin for different cell types. Each study was triplicated for statistical analysis.

2.4. Effects of GaM on cell behavior

2.4.1. Proliferation

To evaluate the effect of GaM and gentamicin sulfate on cell proliferation, hDFs were seeded on a 96-well plate at an initial seeding density of 2k cells/well and left undisturbed for 24 h before treatments. GaM-conditioned culture media at concentrations of 25, 50, and 100 μM were used to treat hDFs for 24–72 h. Untreated cell grown on TCPS was used as a blank control. Before the treatment and 1, 2, and 3 days after treatments, hDF cell densities were determined with PicoGreen® fluorescence assay following the manufacturer's instruction. Each study was triplicated for TCPS and each concentration of GaM.

2.4.2. Collagen synthesis

The effect of GaM on collagen type I synthesis by fibroblasts was characterized based on the immunofluorescence method adopted from a previous study [40]. HDFs were seeded in a 48-well plate at 30,000 cells/well density and cultured for designated periods of time. Blank, 25 μM GaM-conditioned, and 50 μM-conditioned culture media were added to treat hDFs and changed every three days throughout the course of the study. At days 1, 3, 7, 10, and 14, after fixation with 10 % neutral buffered formalin (VWR, Radnor, PA), cells were then washed with PBS and incubated with 0.5 ml readily prepared 0.1 wt% Pico-Sirius Red (PSR) solution for 24 h. The dye solution was carefully removed from each well, and wells were rinsed with DI water until the washing fluid was colorless. The PSR fluorescence intensities (ex 561 nm/em 635 nm) were read to quantify the relative collagen production levels by normalization with the initial collagen content on day 0. The well plate was then dried for 24 h for stereoscope (3X) and microscopy (4X) imaging for qualitative analysis.

2.5. GaM-loaded PLGA microsphere fabrication

The fabrication of GaM-loaded PLGA microspheres was based on the electrospraying technique. GaM and PLGA (50:50, ester terminated; Lactel Absorbable Polymers) were first dissolved in dichloromethane at pre-determined concentrations. GaM-loaded PLGA microspheres were fabricated by electrospraying the solution at a designated parameter set, including the flow rate, charge, needle gauge, and distance to the collection plate (Supplemental Table 2). The microspheres of different particle sizes (diameters of 2, 4, and 6 μm) and with different GaM loading mass ratios (15 %, 25 %, and 37.5 %) were fabricated and then imaged with scanning electron microscopy (SEM) (Phenom Pro; Nano-Science Instruments, Phoenix, AZ). Images were captured at magnifications of 1000x, 2500x, 5000x, 7500x, and 10000x. The average microsphere size was then determined in MATLAB associated with Image J with the 2500x image, Supplemental Fig. 3. Briefly, a MATLAB script was created to differentiate and outline all the surface microspheres to calculate the microsphere diameters based on their area from the SEM images. Three individually fabricated specimens were collected for each microsphere composition, and at least five different points on one specimen were analyzed.

2.6. Fabrication and characterization of GaM-loaded hydrogel foam

2.6.1. Fabrication of the GaM-loaded hydrogel foam

Firstly, Poly(Ethylene Glycol) Diacrylate (PEGDA) 6 kDa was synthesized using a method adapted from previous studies [41]. The precursor solution of the hydrogel foam was made by adding 25 wt% PEGDA 6 kDa, 18.75 wt% Pluronic F68, and 4.65 wt% TMPTA to DI water [37]. The precursor solution was then incubated in a 37 °C incubate shaker for 24 h for complete dissolution. Photoinitiator Lithium phenyl-2,4,6-trimethylbenzoylphosphinate (LAP) was dissolved in the precursor solution at 1 wt%. GaM-loaded PLGA microspheres of different compositions were added to the solution to form a uniform mixture at varied microsphere concentrations. Specifically, 75 mg GaM-loaded PLGA microspheres were added to 1 ml hydrogel foam precursor solution, including 2 μm-15 % GaM MS, 2 μm-25 % GaM MS, 2 μm-37.5 % GaM MS, 4 μm-25 % GaM MS, and 6 μm-25 % GaM MS. For varied concentrations, 37.5 mg and 150 mg 6 μm-25 % GaM MS were added to 1 ml hydrogel foam precursor solution compared to previous 75 mg. The precursor solutions were then mixed with air at a specific ratio (solution: air = 1:3) and turned into foams with the lab-developed syringe foaming procedure. The foam was then placed between 3 mm spacer plates and crosslinked for 15 min under UV light (365 nm) while dry ice was added nearby the hydrogel foam to maintain a curing temperature of 15 °C. The cured foam was added with a designated volume of DI water and swelled for 8 min for equilibrium hydration. Finally, the hydrogel foam was freeze-dried for 24 h, followed by ethylene oxide sterilization for 24 h.

2.6.2. Characterization of the GaM-loaded hydrogel foam

The fabricated hydrogel foam was trimmed to foam stripes, and the foam cross-section was imaged with SEM (260x and 2500x) to demonstrate the microsphere encapsulation. Three 6 mm disks were punched from the hydrogel foam with a biopsy punch and weighed as the first initial specimen weight, $m_{specimen,1}$. The theoretical GaM loading of each foam disk was estimated by:

$$m_{GaM,specimen} = m_{specimen,1} \times \frac{m_{GaM,total}}{m_{foam}} \quad [1]$$

where $m_{GaM,\ total}$ and m_{foam} represented the total GaM loading mass and the total mass of the whole GaM-loaded hydrogel foam. The hydrogel foam disk was then soaked in dichloromethane (DCM) for 24 h to dissolve the total GaM content. The total GaM loading mass ($m_{GaM,\ loading}$) was then determined by detecting the optical density of the hydrogel foam DCM extraction at $\lambda = 322$ nm. The standard curves of GaM in DCM solutions with different GaM loading ratios were plotted in Supplement Fig. 4. GaM loading efficiency ratio (%LE) was calculated as:

$$\%LE = \frac{m_{GaM,loading}}{m_{GaM,specimen}} \times 100\% \quad [2]$$

After removing DCM, hydrogel foam was dried for another 24 h and weighed to obtain the second dry weight, $m_{specimen,2}$. Assuming that DCM extracted the PLGA polymer, surfactant, and uncross-linked macromer, the dried hydrogel foam disk contained only crosslinked PEGDA and TMPTA network. The initial polymer content before curing was derived by correcting the initial hydrogel foam specimen weight ($m_{specimen,1}$):

$$m'_{specimen,1} = m_{specimen,1} \times \frac{m_{foam} - m_{GaM,total} \times \%LE}{m_{foam}} \times \frac{MF_{PEGDA} + MF_{TMPTA}}{MF_{PEGDA} + MF_{TMPTA} + MF_{F68}} \quad [3]$$

where MF_{PEGDA}, MF_{TMPTA}, and MF_{F68} represented the mass fractions of different components in the hydrogel foam precursor solution. Therefore, the hydrogel foam gel fraction was calculated by:

$$\%gel\ fraction = \frac{m_{specimen,2}}{m'_{specimen,1}} \times 100\% \quad [4]$$

2.6.3. GaM release from the GaM-loaded hydrogel foam

To profile the GaM release, the GaM hydrogel foam was trimmed into specimens of 15 × 15 mm and placed on a lab-made semipermeable device, simulating the one-direction release from the foam to 6 ml DI water, Fig. 6A. Particularly, dialysis tubing was trimmed into a 40 × 40 mm square single-layered membrane. The membrane was placed between two 3D-printed frames with inner square holes, allowing for solution exchange. The excess edges of the membrane were then folded upwards, and two designed caps locked the frames and the membrane to secure the sealing. The assembly was placed in a 35 mm petri dish before a hydrogel foam specimen was positioned on the membrane, and DI water was added to fill the space underneath the membrane. The GaM release was conducted at room temperature, and the releasate was collected at the designated time point and replaced with 6 ml fresh DI water for seven days. The GaM concentration was detected by measuring the solution's optical density at 306 nm, compared to a standard concentration curve. The cumulative GaM release percentage was derived by normalizing the absolute release amount to the actual loading mass derived from the last part.

2.7. In vitro evaluation of GaM-loaded hydrogel foam

2.7.1. Cytotoxicity

2 μm-37.5 % GaM MS hydrogel foam was selected for the following *in vitro* and *in vivo* evaluations. The biocompatibility of the GaM-loaded hydrogel foam was confirmed by treating wound-related hDFs. The hDFs were cultured in 12-well plates at an initial density of 100,000 cells/well and incubated at 37 °C for 24 h without disturbance. GaM-loaded hydrogel foam specimens (d = 10 mm) treated hDFs via Transwell filter inserts for 24 and 72 h. The cell viability was characterized with the aforementioned resazurin assay. TCPS and 70 % ethanol treatments were used for positive and negative controls. The live/dead viability kit labeled the live cells with calcein-AM and the dead cells with ethidium homodimer-1. Fluorescence images were sequentially taken to discriminate the live and dead cells after different treatments.

2.7.2. Antimicrobial efficacy

The Kirby Bauer disk diffusion assay was employed and adjusted to evaluate the antimicrobial activity of the GaM-loaded hydrogel foam as previously described [38]. Briefly, GaM-loaded or blank hydrogel foam was punched into 6 mm diameter disks and UV sterilized for 4 h on each side. MSSA 29213 inoculum or MRSA 43300 inoculum was prepared and then spread onto RPMI agar. GaM-loaded and blank hydrogel foam specimens were then placed on the inoculated RPMI agar plate with blank WhatmanTM #1 paper filter disks (diameter of 6 mm) used as negative controls. Paper filter disks loaded with 60 μg vancomycin hydrochloride were used as positive controls. After incubating the agar plate at 37 °C for 24 h, the picture of the agar plate was recorded for visualization. Two 8 mm cylindrical disks were then punched from the agar plate right underneath the applied treatment samples. The punches were then transferred to 2 ml microcentrifuge tubes and added 600 μl RPMI media. Bacteria were detached from the punches and resuspended in RPMI media by sonication for 5 min and vortex for 10 s three times. At last, the bacteria suspension was spread on the BHI agar plate to derive the bacteria number on the punched agar disk after different treatments. The tests were triplicated for both MSSA 29213 and MRSA 43300.

2.8. In vivo evaluation of GaM-loaded hydrogel foam

2.8.1. Animals

A previously described equine distal limb wound model was modified for the *in vivo* evaluation of the GaM-loaded hydrogel foam [42]. The protocol for this study was approved by the University's Institutional Animal Care and Use Committee (protocol A2022 05-003-Y2-A1). Sample size calculations revealed that 6 horses were needed. These calculations were performed based on the following assumptions: 1) a significance level of 5 %; 2) statistical power of 80 %; 3) the expected reduction in healing time between treated and control groups and 4) numbers of days it requires for equine distal limb wounds to heal based on a previous work with this model [43]. Horses donated to the University for teaching and research were utilized for this study. All horses were healthy based on physical examination with no evidence of skin injury to the distal forelimbs. Each horse was housed in a 3.7 × 3.7 m stall adjacent to other horses in a research facility with natural light and artificial lighting for the duration of the study.

2.8.2. Surgical wound model

Horses were administered the non-steroidal anti-inflammatory drug (NSAID) flunixin meglumine (1.1 mg/kg IV). General anesthesia was induced with xylazine HCl (1.1 mg/kg IV), midazolam (5 mg/kg IV), and ketamine HCl (3 mg/kg IV) and maintained with a constant-rate infusion of 5 % guaifenesin with 1000 mg ketamine HCl and 500 mg xylazine HCl per liter, administered at 2 ml/kg/h. Horses were positioned in dorsal recumbency and forelimbs were suspended. The forelimbs were clipped circumferentially from the distal carpus to the distal metacarpophalangeal joint. Aseptic preparation was performed with chlorhexidine and alcohol in a routine manner. A sterile 2.5 × 2.5 cm template was used to create 4 wounds of 6.25 cm^2 on the dorsolateral aspect of each metacarpus, evenly distributed between the proximal aspect of the metacarpophalangeal joint and the distal aspect of the carpus such that 2.5 cm of normal skin remained between each wound. Full-thickness incisions were made, and the excised skin was bluntly dissected off the subcutaneous tissues, Fig. 8A. Following removal of the skin, a routine distal limb bandage was applied prior to recovery from anesthesia (study day −7). Bandages were changed every 3 days for the duration of the study. Seven days after wound creation all wounds were monoinoculated with 5×10^7 CFUs MRSA (ATCC 43300), study day 0, Fig. 8B. The wounds were left untreated for 2 days before the treatment

with blank or GaM-loaded hydrogel foam specimens. These hydrogel foams were loaded with 75 mg/ml 2 μm-37.5 % GaM microspheres and blank hydrogel foams were fabricated. All foams were trimmed into 3 × 3 cm specimens and sterilized with ethylene oxide. Both blank and GaM-loaded hydrogel foams were submerged in 1.6 ml PBS to reach a 50 % pre-hydration level immediately prior to application. The foams were placed directly on the wounds and covered with a non-adherent gauze followed by a semipermeable dressing (Tegaderm®). These were secured with a sterile roll gauze (Kling® Medline). This inner sanctum was then sealed with an adhesive layer (Lightplastpro®, BSN Medical, Hamburg, Germany) followed by a standard distal limb bandage. The hydrogel foam treatments were changed every three days. A biopsy was obtained from each wound on days 2,7,14, and 21 as previously described. Briefly, a 3 mm disposable punch biopsy (Disposable Biopsy Punch, Integra Miltex, York, Pennsylvania, USA) was used to obtain a sample of the wound bed to a depth of 5 mm. The resulting sample was weighed in a preweighed tube containing 1 ml sterile DPBS and 7 glass beads (3 mm glass beads, VWR International, Radnor, Pennsylvania, USA). The tissue was homogenized by bead beating for 20 s at 4.85 m/s prior to performing quantitative culture and DNA isolation (see below).

2.8.3. Treatment efficacy

To characterize the wound healing outcome and the efficacy of GaM-loaded hydrogel foam in controlling infection, the wound size, total bacterial bioburden, and *S. aureus* bioburden were quantified on Days 2, 7, 14, and 21, Fig. 8B. Microscopic pathology scores were obtained from tissue collected on day 21.

Wound area: The height and width of each wound were measured in triplicate on days Days 2, 7, 14, and 21 with a digital caliper (Mitutoyo Corp., Model CD-12″ASX, Mitutoyo Corporation, Aurora, Illinois, USA) and area determined from the average of those measurements.

MRSA Quantification: For MRSA quantification via qPCR, DNA was isolated from the remaining homogenate using a commercially available kit (QIAamp DNAStool Mini Kit, Qiagen, Düsseldorf, Germany) according to manufacturer's protocol and qPCR for the gene conferring oxacillin resistance (*mecA*) and *S. aureus*-specific gene sa442 performed as previously described [42,44]. Standard curves were included in every run to allow quantification of the number of bacteria present in the original sample. Each standard curve consisted of serial 10-fold dilution series of DNA from *S. aureus* (ATCC29213) or serial 10-fold dilution series of DNA from *S. aureus* (ATCC43300). Negative controls consisted of *S. pseudintermedius* DNA from a clinical isolate as well as a negative control without template DNA added to the reaction mixture. Copy numbers of each gene per gram of tissue were then generated.

Total bioburden: The amount of total bacteria in wounds was determined quantifying copy numbers of the 16S rRNA gene per gram of tissue. Standard curves were included in every run to allow quantification of these gene. Each standard curve consisted of serial 10-fold dilution series of DNA from *Escherichia coli* (*E. coli*) ATCC12435. DNA was isolated from tissue samples as described above. Using the universal 16S rRNA primers 16s_515_F and 16s_806R_mod, sybr based qPCR was performed and copy numbers of the 16S rRNA gene per gram of tissue were generated.

Microscopic Pathology: On Day 21, an end-point biopsy was performed routinely using standing sedation, local anesthesia, and an 8-mm punch biopsy to acquire a biopsy specimen that contained normal surrounding tissue, the wound margin, and the granulation bed. To assess the wound histology, biopsy specimens were scored semi-quantitatively blinded to the treatment groups as previously described [45]. The scored criteria included exuberant granulation tissue, inflammation, epithelialization, fibroplasia, and angiogenesis. After Day 21, wounds continued to be treated until full recovery as appropriate.

2.9. Statistical analysis

Data averages are accompanied by ± standard deviation unless otherwise stated. Statistical analysis was performed utilizing a standard one-way ANOVA with Tukey's post hoc analysis unless stated otherwise. Statistical significance was accepted at $p < 0.05$. Repeated measures data generated in our *in vivo* study were analyzed with repeated measures ANOVA. Normality was assessed with the Shapiro-Wilk test, and data were transformed as appropriate to meet statistical assumptions. Post-hoc comparisons were performed, and the Tukey test was used to correct for a multiplicity of comparisons.

3. Results

3.1. Bacterial and cellular responses to GaM

3.1.1. Antimicrobial activity of GaM, gentamicin, and vancomycin

This work employed an improved microdilution assay to determine the post-treatment bacterial density with quantitative analysis of the bacterial suspension's optical density (turbidity) and CFU counting. MSSA 29213 was treated by a series of GaM concentrations from 250 to 15000 μM, resulting in different bacteria densities after 24 h, Fig. 1A. As the GaM concentration increased, the difference in optical density of bacterial inoculum before and after treatment decreased, demonstrating the growing inhibitory effect on bacteria growth. The CFU counting result indicated that 750 μM was the lowest GaM concentration that reduced the bacterial density to below the initial seeding density (5×10^5 CFU/ml) and identified as the GaM MIC against MSSA 29213. Also, a GaM concentration of 4000 μM eliminated over 99.9 % of the initial inoculated bacteria, making out the GaM MBC. Similarly, MIC and MBC of GaM against methicillin-resistant strain MRSA 43300 were characterized as 750 μM and 5000 μM, respectively, Fig. 1B. In comparison with GaM, two clinically applied antibiotics, gentamicin and vancomycin, were evaluated in terms of their MIC and MBC against these two *S. aureus* strains by the same characterization method. The MIC/MBC of gentamicin against MSSA and MRSA were determined as 1 μM/2 μM and 2000 μM/4000 μM, Fig. 1C and D. For vancomycin, MIC/MBC against MSSA and MRSA were determined as 1 μM/2 μM and 10 μM/25 μM.

3.1.2. Cytotoxicity of GaM, gentamicin, and vancomycin

The cytotoxicity of each antimicrobial agent was characterized by evaluating the hDF viability after treatments. This study treated hDFs with antimicrobial agent-conditioned growth media at a series of concentrations ranging from 25 to 15000 μM. The fibroblasts showed lower cell viability after being treated with higher GaM concentrations with IC_{50} identified as 2220 ± 590 μM, Fig. 2A, respectively. Gentamicin's IC_{50} for hDF was identified as 5770 ± 2030 μM while vancomycin's IC_{50} was 400 ± 85 μM, Fig. 2B–C, respectively. It was noted that the relative hDF viability at high GaM concentrations approached 50 %, while gentamicin and vancomycin of high concentrations induced more cell death and demonstrated higher cytotoxicity. With the IC_{50} for hDF identified, the selectivity indices were derived for different antimicrobial agents, showing the highest selectivity index of vancomycin at 36.0 ± 7.0, followed by GaM's 3.0 ± 0.8 and gentamicin's 2.0 ± 0.3.

3.1.3. Effect of GaM on cell behavior

Cellular responses to GaM were characterized regarding its effects on hDF proliferation and cell collagen synthesis. Over the three days of different treatments, both 25 μM and 50 μM GaM groups showed comparable proliferation trends as the TCPS group. However, treated with 100 μM GaM, hDF proliferation slowed down after Day 1 and showed no increment in cell number from Day 2 to Day 3. Collagen synthesis by hDFs was characterized semi-quantitatively with the PSR fluorescence intensities and qualitatively with the staining results. According to the Pico-Sirius Red fluorescence intensity, the collagen content of TCPS and 25 μM GaM increased to three times the initial collagen content over two weeks, Fig. 3B. In contrast, the 50 μM GaM-treated hDFs demonstrated a smaller increment in collagen synthesis after Day 3 and a reducing collagen content after Day 7. In the stereoscopic images, deposited

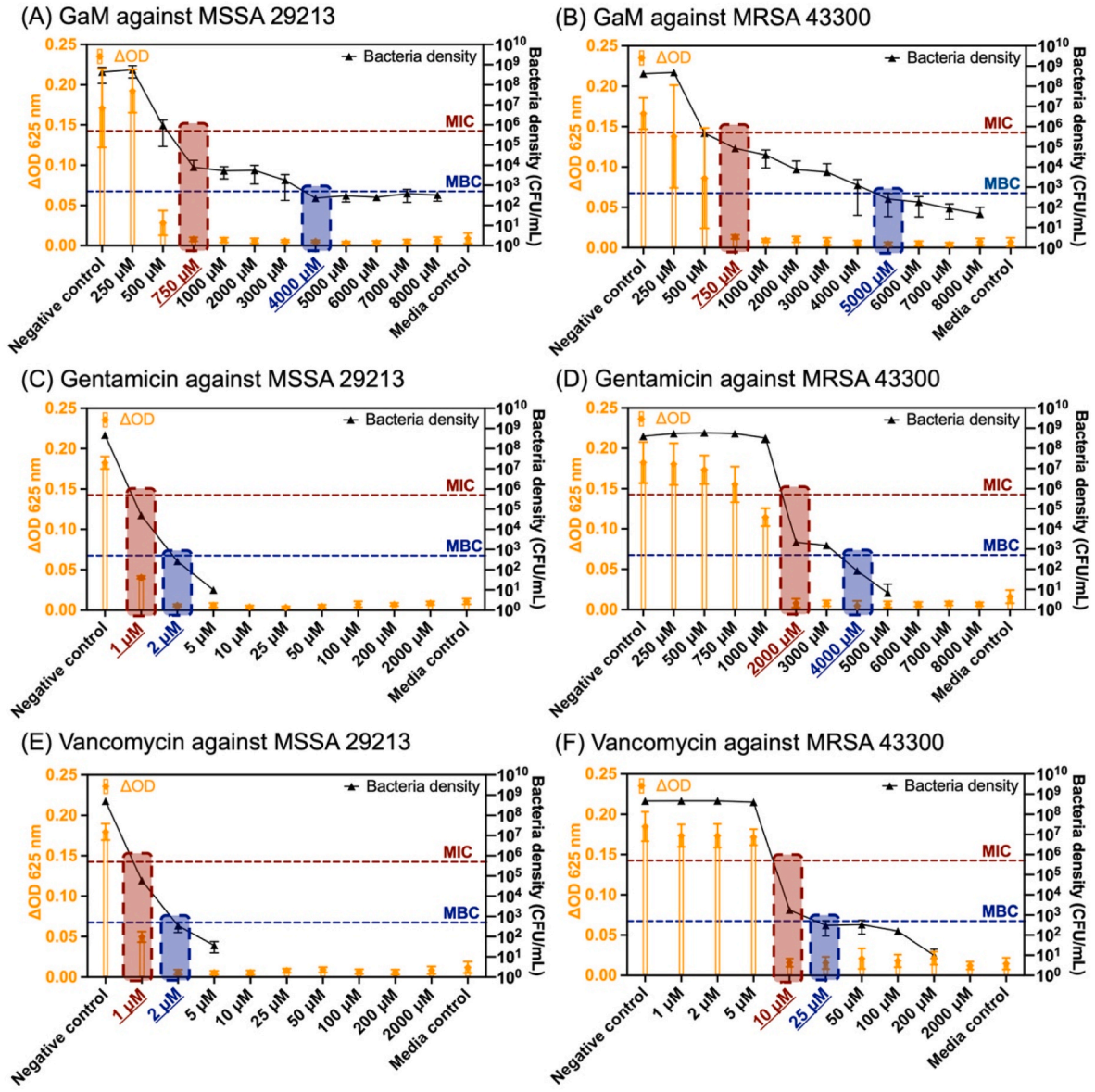

Fig. 1. Bacterial inhibitory and bactericidal concentrations of antimicrobials against MSSA (non-resistant strain: 29213) and MRSA (resistant strain: 43300). The optical density of the bacterial culture suspension and the bacterial density (in CFU/ml) after treatment by different concentrations of antimicrobials: (A) GaM against MSSA 29213; (B) GaM against MRSA 43300; (C) gentamicin against MSSA 29213; (D) gentamicin against MRSA 43300; (E) vancomycin against MSSA 29213; (F) vancomycin against MRSA 43300. MIC was denoted in red and MBC in blue.

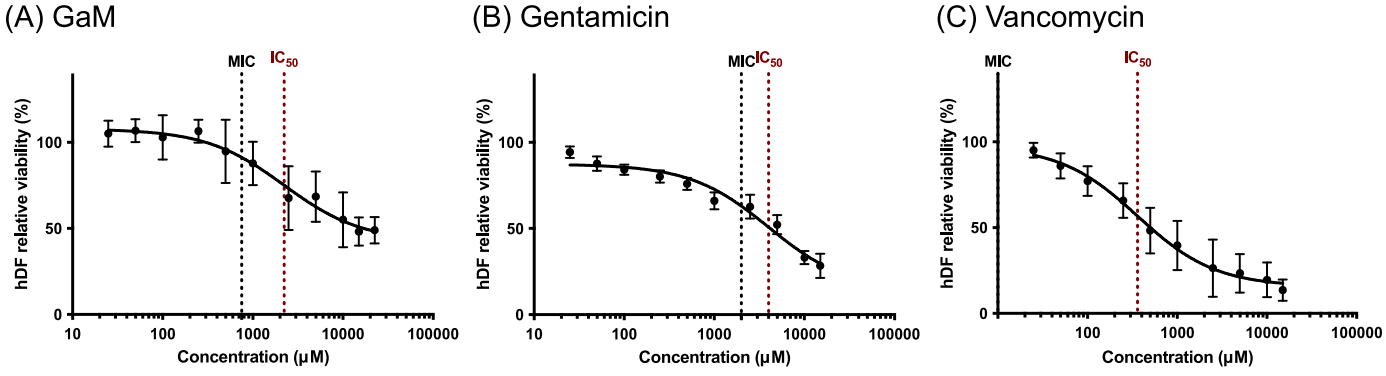

Fig. 2. The dose effects of different antimicrobial agents on the hDF viability: (A) GaM; (B) gentamicin; (C) vancomycin.

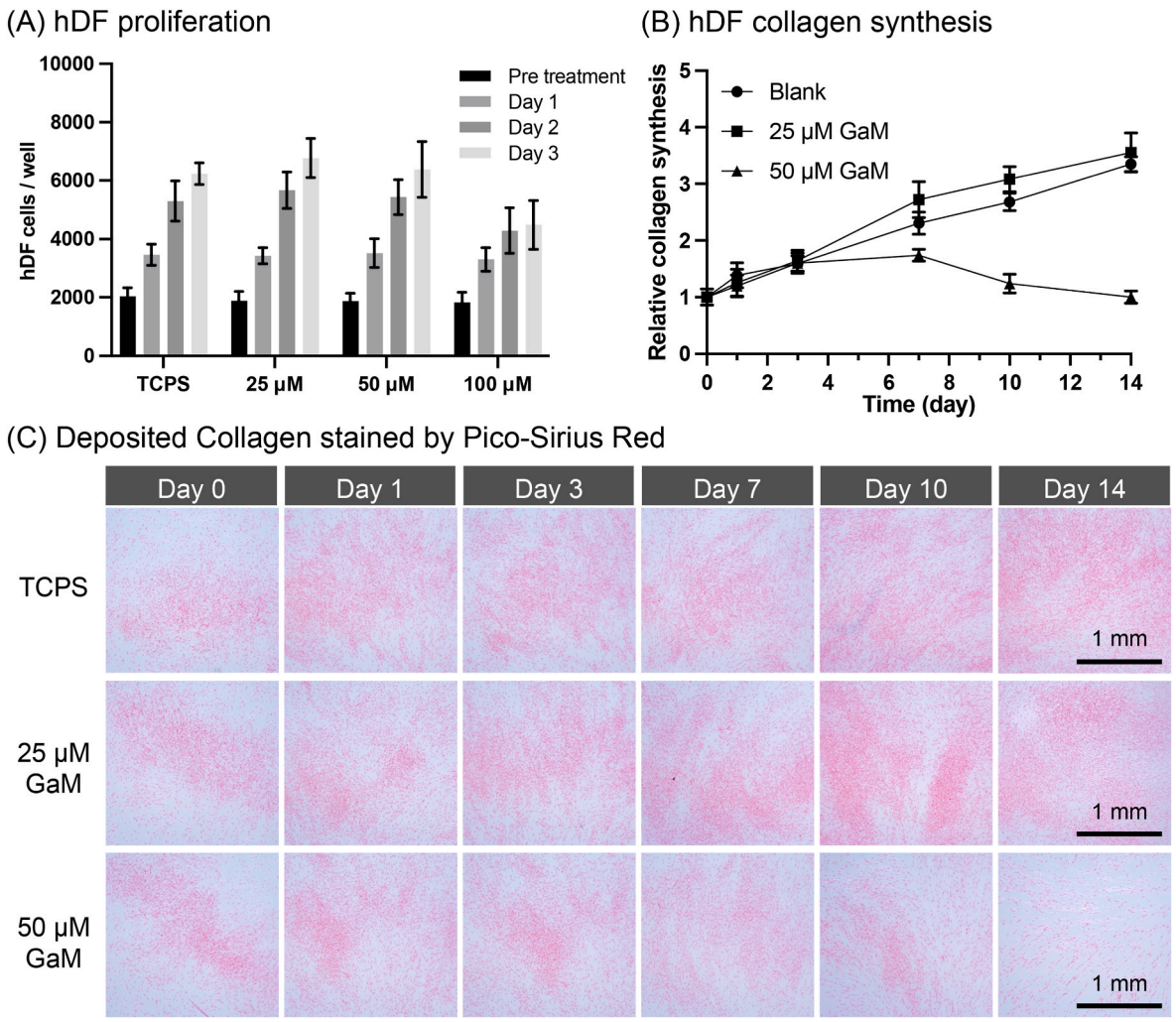

Fig. 3. (A) The dose effect of GaM on the hDF proliferation. (B) The effect of GaM on collagen synthesis by hDFs over 2 weeks. (C) Pico-Sirius Red staining of synthesized collagen by hDFs.

collagen was stained by red dye, showing similar trends of collagen content to the fluorescence intensity results, Fig. 3C. In addition, microscopic images of the fixed hDFs were taken and represented the hDF cell densities of different groups at each time point, Supplemental Fig. 1. As hDFs were seeded at high density initially, they displayed high confluency in almost all images except for the 50 μM GaM group on Day 14. By comparing Day 14 and the previous time point, about 50 % of hDFs were detached with 50 μM treatment.

3.2. Fabrication and characterization of GaM-loaded PLGA microspheres

3.2.1. Electrospraying and modulation of GaM-loaded PLGA microspheres

GaM-loaded PLGA microspheres with target sizes of 2,4, and 6 μm and GaM concentrations of 15 %, 25 %, and 37.5 % were fabricated via electrospraying, Fig. 4A. The GaM loading of the microspheres, i.e., 15 %, 25 %, or 37.5 %, was determined by the GaM mass ratio with respect to the total microsphere mass (GaM + PLGA). Moreover, the electrospraying solution viscosity, the solution flow rate, and the needle gauge were adjusted to acquire varied microsphere sizes (2, 4, and 6 μm). The electrospraying parameters for different microspheres were detailed in Supplemental Table 2. The electrospraying solution viscosity was determined mainly by PLGA concentration in the precursor solution as the precursor solution became more viscous with a higher PLGA concentration, Supplemental Fig. 2A. However, it did not significantly change with varying GaM concentrations, Supplemental Fig. 2B.

Fabricated microspheres were imaged with SEM, and their size distributions were profiled utilizing a MATLAB-powered script for image analysis, Supplemental Fig. 3. Microspheres of 2, 4, and 6 μm diameter with 25 % GaM loading showed mostly spherical shapes with a few rod- and pebble-like shapes, Fig. 4B. The average diameters of the microspheres were characterized as 2.30 ± 0.68 μm, 4.24 ± 1.33 μm, and 5.84 ± 1.67 μm. Among them, 6 μm GaM-loaded PLGA microspheres showed two different peaks, with one at around 3 μm and the other larger than 6 μm. Additionally, a series of 2 μm microspheres were fabricated with varied GaM mass loading, i.e., 15 %, 25 %, and 37.5 %, Fig. 4C. The spherical shape was dominant in the morphology of these microspheres. The size distributions were profiled as 2.59 ± 0.70 μm (15 %), 2.30 ± 0.68 μm (25 %), and 2.29 ± 0.47 μm (37.5 %) with similar average sizes and standard error of means.

3.3. Controlled GaM release from antimicrobial hydrogel foam

3.3.1. Fabrication and characterizations of GaM-loaded hydrogel foam

Before characterizing the GaM release profiles, different microspheres with varied sizes and GaM loading were incorporated in porous hydrogel foams, Fig. 5A. The cross-section SEM image of the hydrogel foam displayed that GaM-loaded PLGA microspheres were incorporated into the hydrogel wall while preserving their spherical forms, Fig. 5B. GaM-loaded hydrogel foams with different microsphere compositions and concentrations were characterized, and all types of hydrogel foams

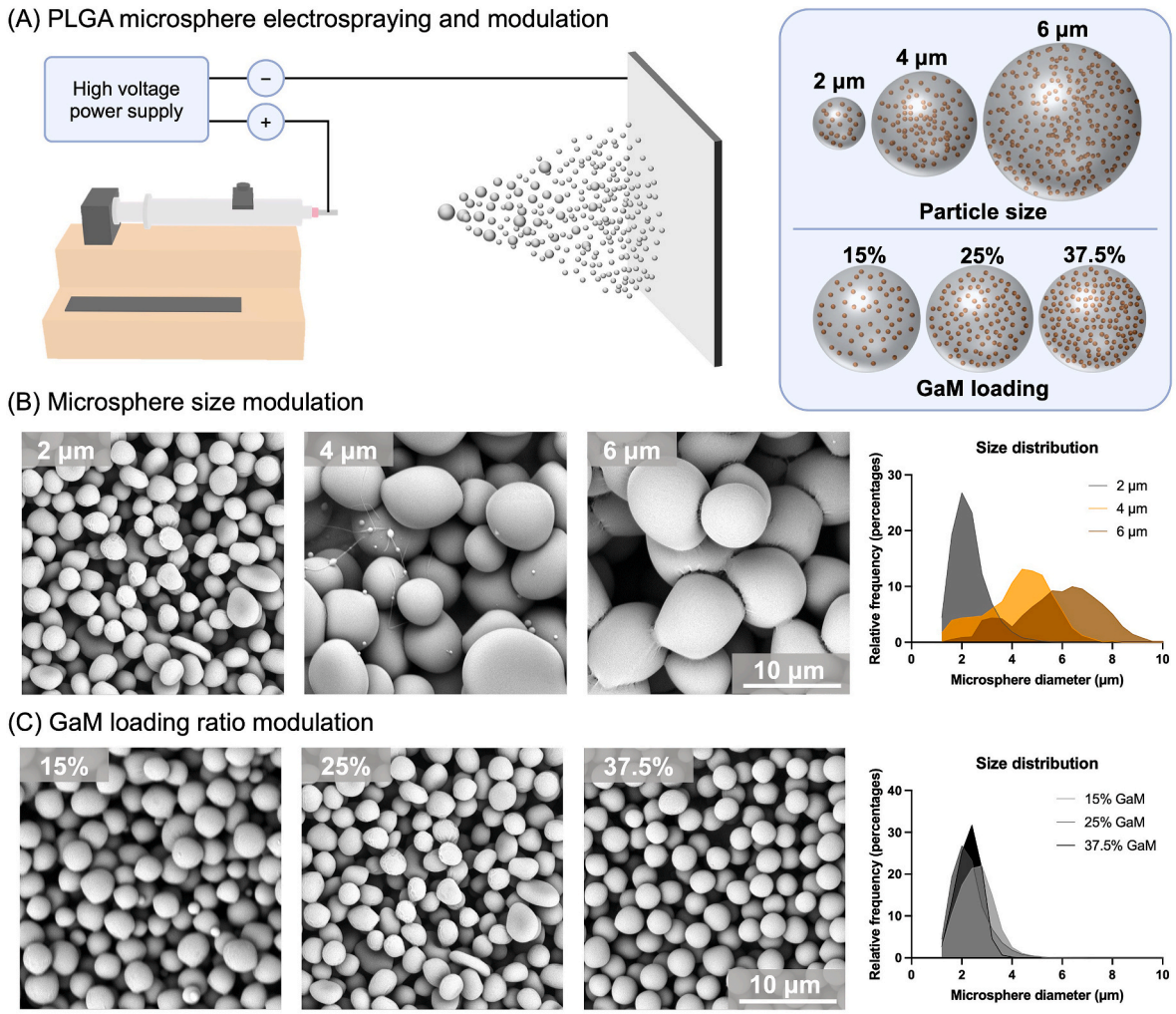

Fig. 4. Fabrication and modulation of GaM-loaded PLGA microspheres. (A) Schematic of GaM-loaded PLGA microsphere fabrication by Electrospraying and modulation of microspheres particle size and GaM loading ratio. Representative SEM images of GaM-loaded microspheres with (B) different sizes and (C) GaM loading ratios.

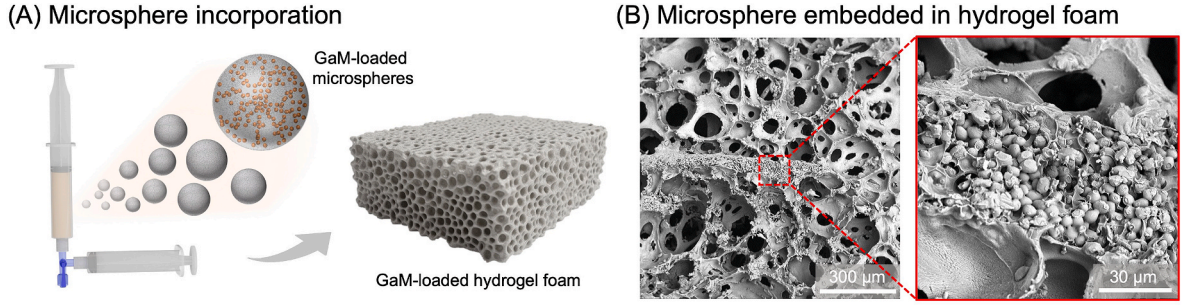

Fig. 5. Fabrication and characterization of GaM microsphere-incorporated hydrogel foam. (A) Schematics of microsphere encapsulation in the PEGDA hydrogel foam. (B) Representative SEM images of hydrogel foam porous structure and microsphere encapsulation.

demonstrated high gel fractions (>95 %) and high GaM loading efficiencies (>90 %), Table 3.

3.3.2. *GaM-loaded hydrogel foam release profiles*

A custom semi-permeable release model was used to detect the GaM release from the GaM-loaded hydrogel foam, Fig. 6A. The GaM release profiles included the accumulated release percentages and daily release amounts of GaM from the hydrogel foams over 7 days. For varying microsphere sizes with the same 25 % GaM loading in the microspheres, the foam with 2 μm microspheres showed a relatively high burst release and released over 55 % of the total GaM within day 1. The GaM first-day burst release decreased with a larger microsphere size as 4 μm MS foams released more than 40 % of the total GaM, and 6 μm foams delivered about 25 %. For 2 μm and 4 μm foam groups, the daily GaM release decreased from day 1 to day 7 when their cumulative release percentage reached around 90 % on day 7. In contrast, the continuous GaM release from 6 μm foams was lower than the first-day burst release but kept relatively constant and higher than the other two groups from day 2–7.

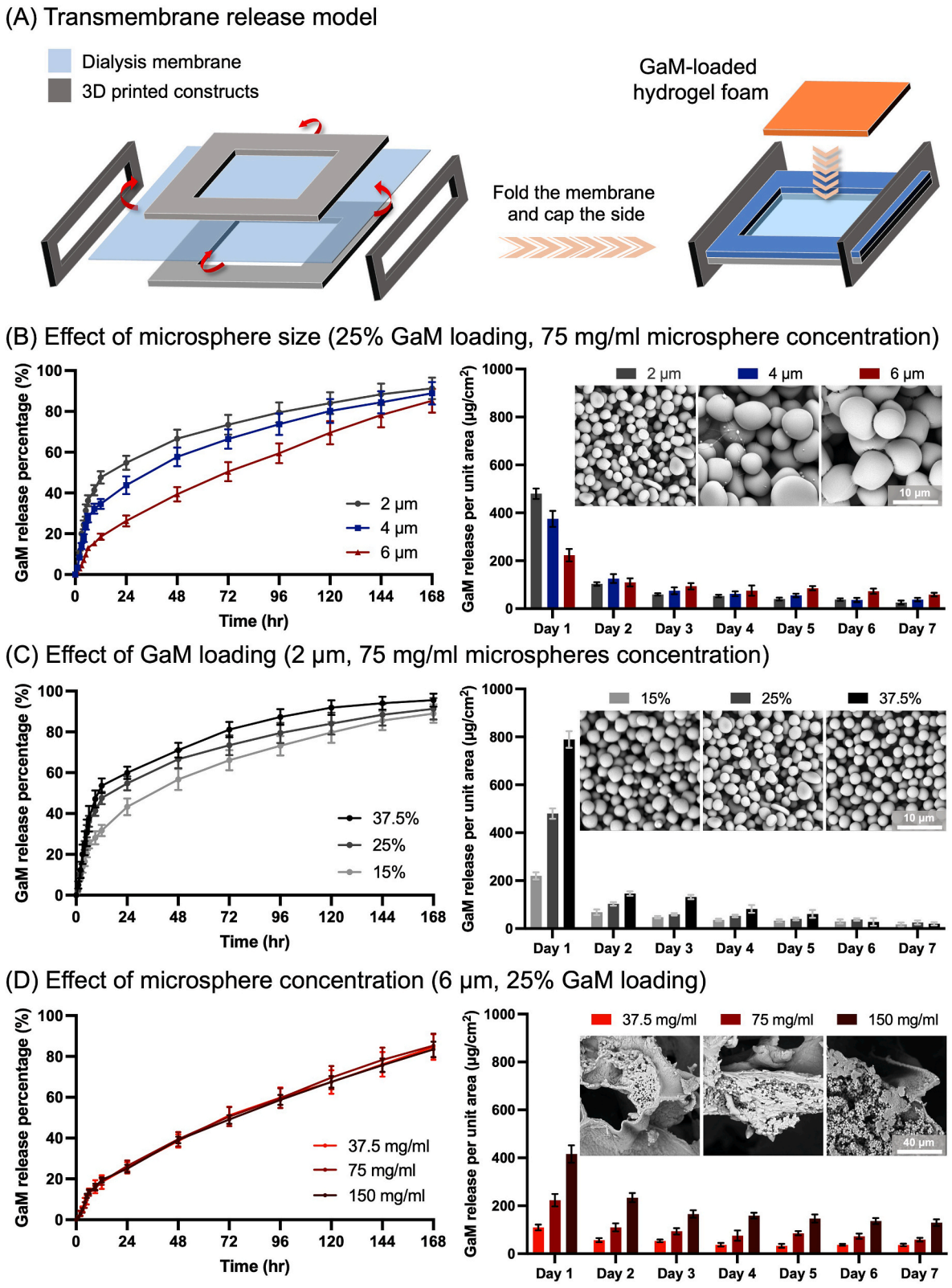

Fig. 6. Controlled release of GaM from hydrogel foams. (A) Schematics of the transmembrane release model to mimic the GaM delivery to wound interface. Modulation of GaM release profile by changing (B) microsphere size, (C) GaM loading mass ratio, and (D) microsphere concentration of the GaM-loaded hydrogel foam.

Microspheres with 15 %, 25 %, and 37.5 % GaM loading also exhibited different GaM release profiles. The GaM burst release decreased as the GaM loading mass ratio decreased from 37.5 % to 15 %. Foams with 2 μm–37.5 % GaM MS released 60 % loaded GaM within 24 h and about 90 % within 5 days. Foams with lower GaM loading MS released over 85 % GaM after 7 days of application. The daily GaM release from 37.5 % GaM foams was the highest among the three groups until day 6. However, 25 % GaM hydrogel foams were constantly higher than 2 μm-15 % GaM MS one over 7 days. Hydrogel foams with different concentrations (37.5, 75, and 150 mg/ml) of 6 μm–25 % GaM microspheres showed similar release profiles. And the GaM release amounts each day increased proportionally with increased microsphere concentration.

3.4. In vitro and in vivo evaluations of GaM-loaded hydrogel foam

3.4.1. Cytotoxicity and antimicrobial efficacy

GaM-loaded hydrogel foam with 2 μm–37.5 % GaM was selected for further evaluation as it met the bactericidal concentration with a high burst release and sustained antimicrobial activity for the target 5 days. HDF viability after 24- and 72-h treatments by GaM-loaded hydrogel foam was greater than 90 %, indicating excellent cytocompatibility.

To verify the antimicrobial activity of GaM-loaded hydrogel foam, the Kirby-Bauer disk diffusion assay was used to obtain the zone of inhibition after treatments with the antimicrobial hydrogel foam. Additional studies were performed to quantify bacterial number in the treatment area normalized to the surrounding plate to confirm antimicrobial activity, Supplemental Fig. 5A. For the MSSA strain 29213, ZOI test results showed that the blank filter disk negative control did not inhibit bacterial growth, Fig. 7B and. The 60 μg vancomycin-loaded filter disk generated a clear zone of inhibition of 25.3 ± 0.3 mm. The GaM-loaded hydrogel foam did not form a clear zone of inhibition. A zone with no defined edge indicated bacterial sensitivity to GaM-loaded hydrogel foam. However, the bacterial density results showed that GaM hydrogel foam reduced the bacteria numbers underneath the foam by > 90 % compared to the untreated bacteria counts and negative control. Similarly, for the MRSA strain 43300, the positive control of vancomycin-loaded filter paper formed a zone of inhibition of 25.0 ± 1.5 mm; whereas, the GaM-loaded hydrogel foam did not result in a clear zone of inhibition but reduced the bacteria number by > 90 %, Fig. 7C.

3.4.2. In vivo evaluation of GaM-loaded hydrogel foam

The efficacy of GaM-loaded hydrogel foam in treating equine distal limb wounds was evaluated compared to blank hydrogel foam. Because equine wounds initially retract but do so to different degrees based on individual characteristics such as skin tightness and wound location, wound sizes were different among the horses at the beginning of the treatment period (i.e., day 2). In order to account for that variation, wound size was analyzed by examining the proportion of wound closure relative to day 2. There were statistically significant reductions in wound size within the GaM-loaded hydrogel group over the 21-day treatment period but not in the blank hydrogel group, Fig. 8C. The mean wound size on day 21 for the blank hydrogel group was still 70 % (±40 %) of the day 2 wound size, but GaM-treated wounds were only 40 % (±22 %) of the day 2 wound size ($p = 0.0001$). This difference was not statistically different between the two groups at any given time point likely due to the high variability of blank hydrogel group. Based on these results, the GaM hydrogel foam imparted favorable effects on wound

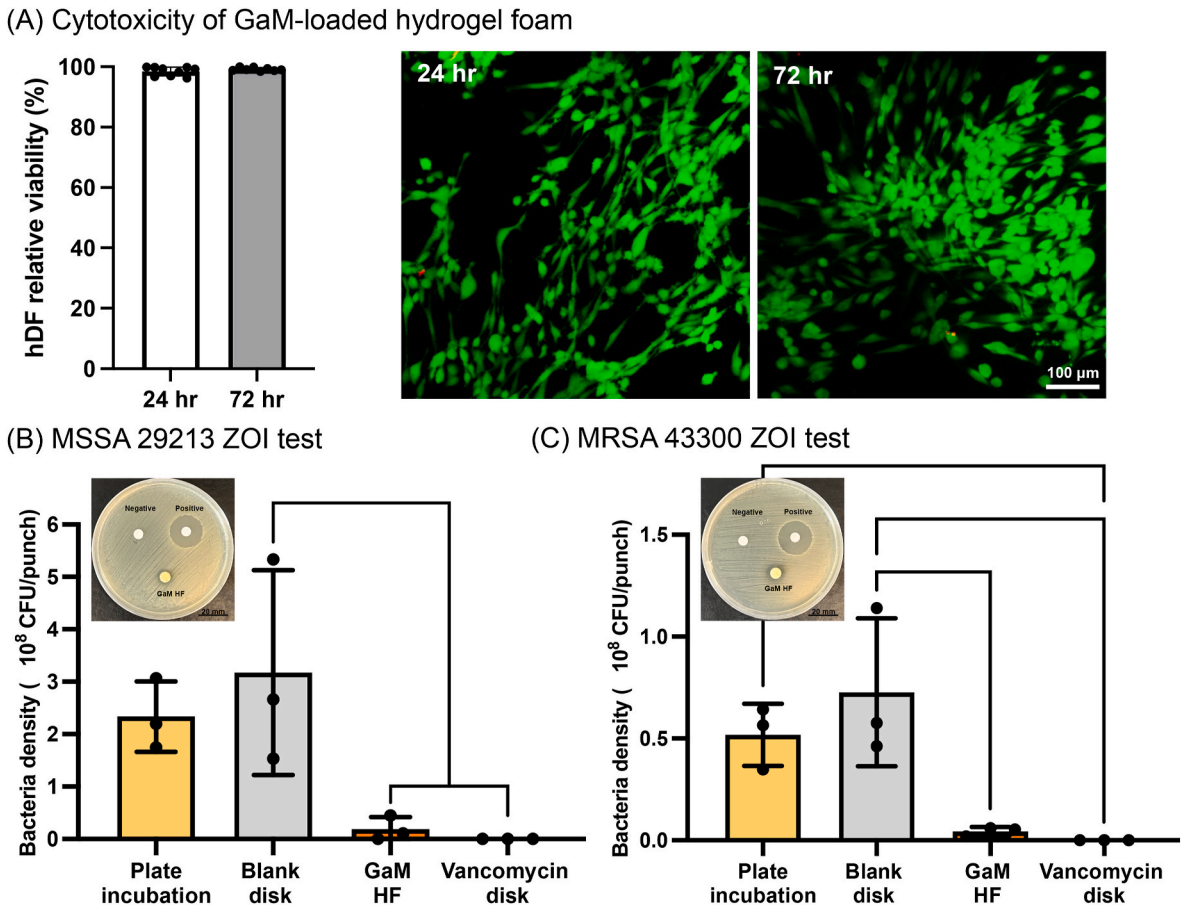

Fig. 7. In vitro evaluation of GaM-loaded hydrogel foam. (A) Cytotoxicity of GaM-loaded hydrogel foam. ZOI test results after different treatments with bacterial counts per 8 mm punch on different bacterial strains: (B) MSSA 29213 and (C) MRSA 43300.

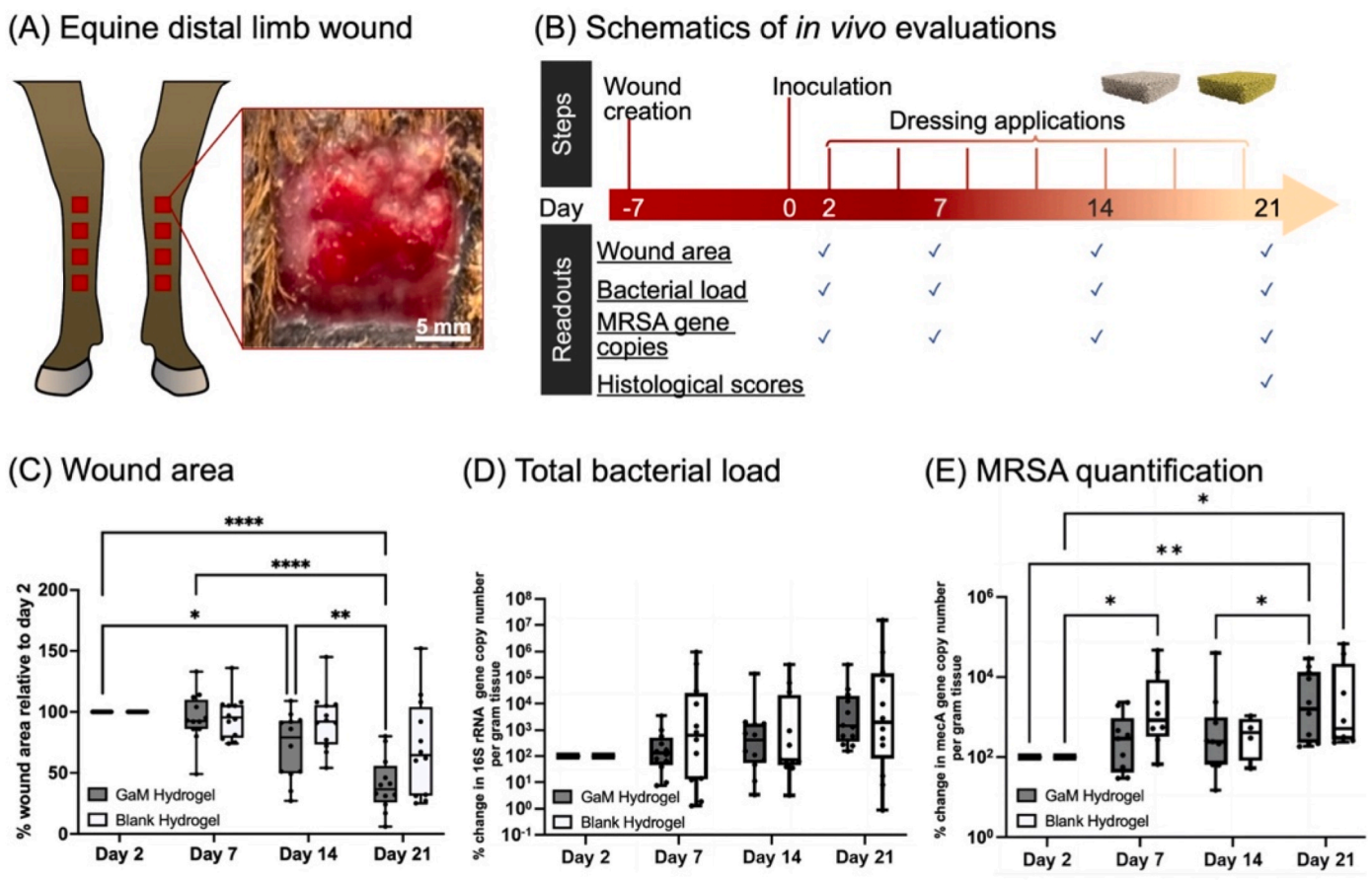

Fig. 8. *In vivo* evaluations of blank and GaM-loaded hydrogel foams. (A) Establishment of the equine distal limb model and a representative wound photo; (B) Schematics depicting animal study details; (C) Wound area change over three weeks after treatments relative to Day 2; (D) Total bacterial load (16S rRNA gene copy number/g tissue); (E) MRSA quantification represented by mecA gene expression levels of existing bacteria.

closure (Supplemental Fig. 8); whereas, the blank hydrogel foam did not significantly reduce wound size.

As with the wound size data, there were considerable differences in the number of bacteria in each wound. For that reason, we analyzed these data relative to day 2. We initially examined the total bacterial load as determined by 16S rRNA gene copy numbers per gram of tissue. The number of bacteria in the wound increased from day 2 to day 21, but there were no significant differences between groups or within groups, Fig. 8D. There were, however, differences in the amount of MRSA between treatments. To ensure our qPCR data for the mecA gene was identifying MRSA and not another species of bacteria with the mecA gene, we compared the abundance of the mecA gene with the *S. aureus* specific gene sa442 and showed that there was near near-perfect correlation and trends thus confirming the mecA qPCR data was accurately reflecting MRSA-specific bioburden, Supplementary Fig. 7. There was no significant increase in the copy numbers of the mecA gene in GaM-treated wounds until day 21. In blank hydrogel wounds, however, there was a significant increase in copy numbers of the mecA gene as soon as day 7. Taken together, these data suggest that there was increased bioburden in both treatment groups, but GaM-treated wounds healed faster and had a lower MRSA-specific bioburden early in the healing process. Interestingly, microscopic pathology scores on day 21 were not different between treatment groups, Supplemental Fig. 9.

4. Discussion

Accompanied by bacterial infection and biofilm formation, chronic wounds are burdened with significant delay and difficulty in healing, thus requiring additional treatments. Bacteria contaminate and colonize the surfaces of chronic wounds from the surrounding skin, external environment, and endogenous sources, leading to critical colonization and eventual infection [46]. Furthermore, most chronic wounds are infected with a mixed bacteria flora, forming a dynamic microbiological environment and leading to the formation of biofilm that encases microbial cells in extracellular polymeric substances [47]. Previous studies have connected bacterial infection and biofilm with excess host inflammation and delayed healing of infected chronic wounds, highlighting the risk of cellulitis, sepsis, and other invasive tissue infections [48–51]. Therefore, many strategies have been developed to control the bacteria growth and proliferation and even eradicate the existing microbial cells [3,8,52]. The methods to control infection and wound management include wound debridement, negative pressure wound therapy, topical and systemic administration of antimicrobial agents, and application of antimicrobial dressings. Wound debridement removes the necrotic, damaged, or infected tissue for wound bed preparation and improves healing outcomes. Debridement can be performed with different methods, such as biological, mechanical, enzymatic, surgical, and autolytic [53,54]. However, traditional debridement methods are limited by associated pain, long treatment period, or allergic reaction [53]. Madhok et al. summarized recently designed debridement techniques of hydrosurgery, monofilament polyester fiber pad, and ultrasound, but further investigation is required to verify their efficacies in treating chronic wounds [55]. For negative pressure wound therapy, there are contradicting results regarding if wound bacterial load increases or decreases after the treatment [56–59]. Furthermore, the administration of antibiotics has been challenged by elevating bacterial resistance and bacterial species- or strain-specific susceptibility [18,19,60]. In particular, methicillin-resistant *S. aureus* has been

recognized as the most prevalent antibiotic-resistant bacterial strain found in chronic wounds.

With high accessibility and cost-effectiveness, antimicrobial wound dressings control wound infection by delivering antimicrobial agents to the wound bed, including silver, iodine, chlorhexidine, and PHMB [61]. However, current antimicrobial agents loaded in the wound dressings are limited by patient sensitivity or allergy to the agents or toxicity. In this work, gallium maltolate (GaM) was applied to treat bacterial infection as a new antimicrobial agent. GaM was first introduced as a chemotherapeutic agent for hepatocellular carcinoma or lymphoma with high oral availability compared to gallium nitrate [62–64]. Several groups then revealed the mechanism of gallium's antimicrobial activity. Gallium can be consumed by bacteria in place of Fe due to their chemical similarity, therefore interfering with all Fe-dependent bacterial metabolism, including DNA synthesis, electron transport, and oxidative stress defense [65]. This study found that gallium inhibited *Pseudomonas aeruginosa* growth and biofilm formation. Another work by DeLeon et al. demonstrated that GaM was capable of eradicating *Pseudomonas aeruginosa* infection in a mouse skin injury model [66]. In 2012, Arnold et al. comprehensively studied the antimicrobial activities of GaM against methicillin-susceptible and resistant strains of *Staphylococcus aureus* as well as methicillin-resistant *Staphylococcus pseudintermedius* [67]. However, previous methods to characterize the minimal inhibitory and bactericidal concentrations of antimicrobial agents are limited to merely the qualitative turbidity of the bacteria inoculum or the measurement of colony forming units after treatment. Also, the initial bacterial inoculation densities varied in different studies, leading to convoluted readout and data analysis [68–70]. Following the guidelines of CLSI M07-A9, a combinatory method of spectrophotometrical reading and colony-forming unit measurement was proposed for a more comprehensive and accurate understanding of GaM's antimicrobial activity [31,38]. Furthermore, no existing study has investigated the development of bacterial resistance to GaM. However, given that gallium hampers Fe-dependent DNA synthesis and other related pathways, the likelihood of bacteria developing resistance to GaM is hypothesized to be minimal.

This work compared the antimicrobial activities of GaM with two commonly used antibiotics, vancomycin and gentamicin, against MSSA 29213 and MRSA 43300. Bacteria were initially inoculated in RPMI at 5×10^5 CFU/ml and treated by different antimicrobial agents at distinct ranges of concentrations. The optical density of the bacteria suspension before and after treatment was read at $\lambda = 625$ nm to determine its turbidity. The change in bacteria inoculum optical density after treatment (ΔOD) was derived by subtracting the initial optical density from the treated one. CFU per volume of the bacterial inoculum was then measured and found to correlate to the optical density values, Fig. 1. For example, MSSA 29213 treated by GaM of 750 μM and higher concentrations showed low ΔOD values and colony-forming units per volume, Fig. 1A. These results demonstrated that the turbidity method was not sensitive and incapable of differentiating low bacterial densities (i.e., $< 10^4$ CFU/ml), confirming the necessity to perform a CFU measurement. The GaM's MICs against both *S. aureus* strains are 750 μM, but GaM MBC against MRSA 43300 was higher than that of MSSA 29213 (5000 vs. 4000 μM), Table 1. In contrast, the gentamicin MIC against MRSA was 2000 times that against MSSA, showing bacterial resistance to gentamicin. Also, gentamicin showed a MIC higher than GaM MIC against MRSA, and therefore a lower efficacy in controlling MRSA infection. Compared to GaM and gentamicin, vancomycin was measured to have much lower MIC and MBC, but MRSA was less susceptible to vancomycin than MSSA. Additionally, the MICs and MBCs of gentamicin and vancomycin against MSSA from this study were similar to the reported values from the literature, Supplemental Table 1 [70,71]. But the MICs and MBCs against MRSA were higher than the reported values, suggesting that difference in measurement methods, different initial bacterial inoculation density, the variance of strain isolates might lead to a discrepancy in results. Also, this work studied hDF viability after treatment by a series of GaM, gentamicin, and vancomycin concentrations and reported the IC_{50} and selectivity index of each antimicrobial agent, Fig. 2 and Table 2. The hDF cytotoxicity of different antimicrobial agents demonstrated an order as vancomycin > GaM > gentamicin, and their selectivity indices ranked as vancomycin > GaM > gentamicin. Although with the highest hDF cytotoxicity, vancomycin had the highest selectivity index and was the most selective for MRSA when treating wound infection, Fig. 2C. Compared to gentamicin, GaM was less toxic at MIC against MRSA, showing a higher selectivity when controlling bacterial infection. In addition, several previous reports showed the antineoplastic activity of GaM or other gallium compounds by disrupting iron-dependent pathways [64,72,73]. Cancer cells, like many rapidly dividing cells, require a considerable amount of iron. Therefore, gallium's interference with iron homeostasis leads to iron deficiency within the cells, causing oxidative stress, impairing DNA synthesis, and ultimately resulting in cancer cell deaths. However, wound cells are less iron-dependent than cancer cells and therefore less sensitive to GaM. With multiple clinical trials of cancer treatment of GaM launched, no severely adverse systemic effects of GaM have been reported. In this work, the GaM IC50 concentration on hDF was determined, providing insights into the safe dosage of GaM. Therefore, GaM demonstrated high potency as an antimicrobial agent that controls bacterial infection without adversely influencing skin cells and the risk of rising bacterial resistance.

The proliferation stage of wound healing comprises several important biological and physiological events, including fibroblast migration and proliferation, extracellular matrix deposition, angiogenesis, epithelialization, granulation tissue formation, and wound contraction [74–76]. Collagens play central roles in wound repair as essential granulation tissue components, providing the structural basis for angiogenesis, wound contraction, and re-epithelialization [77]. Here, the effects of GaM on hDF proliferation and collagen production were characterized to assess GaM's potential in promoting wound healing. 25 μM, 50 μM, and 100 μM GaM were selected due to minimal toxicity to hDF. 25 μM and 50 μM GaM did not significantly impede or promote the hDF proliferation over the 3-day treatment course, but the hDF proliferation slowed in the later 2-day treatment by 100 μM GaM. The hDF collagen production was characterized over two weeks after 25 μM and 50 μM GaM treatments. Fibroblasts treated with 25 μM showed the same increasing collagen content trend as the blank group. In contrast, the

Table 2
MICs, IC_{50}s, and selectivity indices of GaM, gentamicin, and vancomycin.

	MIC against MRSA (μM)	IC_{50} for hDF (μM)	Selectivity index (SI)
GaM	750	2220 ± 590	3.0 ± 0.8
Gentamicin	2000	4010 ± 680	2.0 ± 0.3
Vancomycin	10	360 ± 70	36.0 ± 7.0

Table 1
MICs and MBCs of GaM, gentamicin, and vancomycin against MSSA and MRSA.

Strain	MIC (μM)			MBC (μM)		
	GaM	Gentamicin	Vancomycin	GaM	Gentamicin	Vancomycin
MSSA 29213	750	1	1	4000	2	2
MRSA 43300	750	2000	10	5000	4000	25

Table 3
Gel fractions and GaM loading efficiencies of different GaM-loaded hydrogel foams.

GaM-loaded hydrogel foam	Microsphere composition	Microsphere concentration (mg/ml)	Hydrogel foam gel fraction (%)	GaM loading efficiency (%)
2 μm-15%-75 mg	2 μm-15 % GaM	75.0	95.7 ± 1.8	92.4 ± 1.7
2 μm-25%-75 mg	2 μm-25 % GaM	75.0	95.8 ± 1.7	94.2 ± 1.9
2 μm-37.5%-75 mg	2 μm-37.5 % GaM	75.0	96.0 ± 1.5	94.7 ± 1.5
4 μm-25%-75 mg	4 μm-25 % GaM	75.0	96.2 ± 1.1	93.2 ± 2.3
6 μm-25%-37.5 mg	6 μm-25 % GaM	37.5	95.9 ± 1.6	92.0 ± 3.0
6 μm-25%-75 mg	6 μm-25 % GaM	75.0	95.5 ± 1.9	92.7 ± 1.8
6 μm-25%-150 mg	6 μm-25 % GaM	150.0	96.1 ± 1.7	95.4 ± 1.3

collagen production by 50 μM GaM-treated hDF receded after Day 3. However, the hDF cell density did not decrease until Day 10, suggesting that hDF collagen production ceased after Day 3 with 50 μM GaM treatment. The images of stained collagen display patched collagen depositions on the culture plate, and the collagen content evidently increased over the treatment time, Fig. 3C. Collectively, these results demonstrated that a low concentration of GaM at 25 μM did not adversely affect the wound healing-related hDF behavior. However, GaM MIC of 750 μM, while showing acceptable cytocompatibility, could delay the hDF proliferation and collagen synthesis if it accumulates in the wound. Given that the histological scores showed that GaM-loaded hydrogel foam did not decrease wound fibroplasia or collagen deposition, it was assumed that the released GaM did not accumulate in the wound at levels that impacted collagen synthesis. It was hypothesized that most GaM was consumed by local bacteria and absorption by fluid exchange, resulting in a low GaM concentration in the local wound microenvironment. Despite the limited studies on the GaM pharmacokinetics in cutaneous application, GaM absorption through the wound interface is believed to be rapid due to relatively fast diffusion with its small molecule weight and facilitated blood transport by binding to plasma transferrin after intragastric administration [78,79]. Further investigation is needed to quantify local GaM concentrations in the wound and elucidate the influence of GaM on other biological events in wound healing for a more comprehensive understanding, such as keratinocyte proliferation and migration for re-epithelialization.

The identified MIC and MBC of GaM provided guidelines for a controlled delivery of GaM that could eradicate the existing bacteria with a high burst release and inhibit successive bacteria growth with a sustained supply of GaM without adversely affecting dermal fibroblast cell behavior. In this work, GaM was encapsulated in PLGA microspheres via an electrospraying technique with different microsphere sizes and GaM loading. Among different electrospraying parameters, precursor solution viscosity was shown as the predominant factor in modulating the microsphere size [80]. Specifically, precursor solutions with a high concentration of PLGA (180 mg/ml) were more viscous and resulted in larger average microsphere sizes (4 and 6 μm). The combination of a larger needle diameter and a higher flow rate resulted in a larger volume and increased surface area of liquid droplets, determining the size and surface charge of the Taylor cone and further differentiating 4 and 6 μm [81]. The GaM loading mass ratio did not significantly affect the solution viscosity so microspheres of varied GaM loading could be fabricated with similar microsphere size. We hypothesized that the microsphere size and GaM loading ratio could control the GaM diffusion distance and path, determining its release profile. In particular, a larger microsphere size increased the diffusion distance and required a longer release time, allowing for a more sustained release. In contrast, microspheres with a higher GaM loading ratio had more coherent GaM distribution and more connected drug diffusion channels, enabling faster drug discharge from the microspheres. Different GaM-loaded PLGA microspheres were then incorporated into a porous hydrogel foam to implement an antimicrobial wound dressing for infection control. A hydrogel foam was previously developed to control chronic wounds' moisture balance by providing moisture to dry wounds or removing excessive exudate from discharging wounds [37]. However, the hydrogel foam dressing alone is unable to promote the closure of wounds complicated with infection, necessitating the introduction of antibacterial activity to this wound dressing. The SEM image of the fabricated hydrogel foam composite showed that GaM-loaded microspheres were incorporated into the hydrogel wall. Also, the hydrogel foam gel fractions showed minimal impact by the microsphere incorporation on the foam's curing and structural integrity. The GaM loading efficiencies of different hydrogel foam compositions were also characterized and demonstrated less than 10 % loss of GaM from their theoretical loading amounts, which could be attributed to the unincorporated microspheres during the foaming process. Several measures were taken to reduce the GaM loss, including maintaining the low temperature (15 °C) of the precursor hydrogel foam during the UV-initiated curing and limiting the swelling of hydrogel foam before freeze-drying. UV curing increased the hydrogel foam temperature to near the glass transition temperature of PLGA, changing the GaM diffusivity and polymer phase transition and resulting in a higher burst release in the first 6 h [82]. With these results, this work presented a toolbox for microsphere electrospraying modulation and potentiated controlled drug release by employing microspheres with a specific size, drug loading, and concentrations for target applications.

The hydrogel foam loaded with 2 μm 37.5 % GaM microspheres was later selected for *in vitro* and *in vivo* evaluation. We assessed the *in vitro* cytotoxicity and antimicrobial activity of the GaM-loaded hydrogel foam. Dermal fibroblasts were treated with a GaM-loaded hydrogel foam via a Transwell and demonstrated high viability. In ZOI tests based on the Kirby-Bauer disk assay, GaM-loaded hydrogel foam and filter disk treated MSSA- and MRSA-inoculated RPMI agar plate. First, the blank hydrogel foam formed no zone of inhibition against both MSSA 29213 and MRSA 43300 and there was no observed bacterial inhibitory effects of the hydrogel foam itself, Supplemental Fig. 6. Characterization of bacterial adhesion on the hydrogel foam itself was not performed as bacteria were not expected to adhere to the blank hydrogel foam dressing due to the antifouling properties inherent to PEG hydrogels [83]. The GaM-loaded hydrogel foam displayed a receding bacterial density from the edge of the foam but no clear zone of inhibition. Quantification of bacterial density under the GaM-loaded hydrogel foam indicated a greater than 90 % reduction in bacterial density. The GaM loading mass in the hydrogel foam was characterized as 262 ± 56 μg equivalent to a concentration of 1110 ± 236 μM assuming a cylindrical release volume (D = 15 mm, T = 3 mm). This concentration exceeded the afore-reported GaM MIC of 750 μM, confirming the bacterial inhibition by the GaM-loaded hydrogel foam. Furthermore, GaM-loaded filter disks were also used to treat MSSA and MRSA zone plates. Likewise, no zone of inhibition was obtained, but the bacterial density dropped to less than 0.1 % of the blank control, meaning that the GaM-loaded disk almost eradicated bacteria. The GaM disk loading was measured as 2267 ± 93 μg with an equivalent GaM concentration of 9614 ± 396 μM that was higher than both GaM MBCs against MSSA and MRSA. This indicated that a higher GaM loading was promising to eradicate the existing bacteria. The ZOI test results also suggested that as GaM inhibited bacteria growth by interfering with DNA synthesis and disrupting bacterial defense against oxidative stress, GaM might require a longer time to exhibit the bacterial inhibitory effect. That resulted in a decreased CFU number but no zone of inhibition as bacteria proliferated before GaM took effect.

Finally, the *in vivo* evaluations of blank and GaM-loaded hydrogel

foam demonstrated that the incorporation and controlled release of GaM in hydrogel foam accelerated wound closure and inhibited the growth of MRSA compared to blank hydrogel foams. The mecA gene has been widely used to differentiate MRSA and MSSA, and the SA gene ubiquitously exists in all *S. aureus* strains [84,85]. Therefore, the combination of mecA and SA gene analysis provided a fast detection of MRSA with high specificity [85]. In this work, the mecA and SA gene expression exhibited high concordance, showing that MRSA predominantly existed in these wounds, thus confirming our model successfully created MRSA-infected wounds in horses. Analysis of these data revealed that while GaM did not impact total bioburden, it did reduce the proliferation of MRSA-specific bioburden until day 21. The increase in MRSA during the wound healing process has been shown before with this model [43] and may reflect the decreasing wound size albeit with a similar overall bacterial load, thus increasing load per gram of tissue. While bioburden is an important wound read-out, ultimately, wound healing is the most critical indicator of wound health. In our study, the average wound size reduction percentage driven by the GaM-loaded hydrogel foam treatment was nearly twice compared to that of blank hydrogel foam. This improved wound healing environment was not reflected by microscopic pathology as histology scores were not different between groups. The fact that we used a narrow (0–4) semi-quantitative histology score approach likely made detecting small differences difficult. A future study incorporating a more thorough evaluation of the healing events and cell activities in the future is warranted to elucidate mechanisms by which GaM improved wound healing. One additional factor that may have reduced the efficacy of GaM in our equine distal limb model was the fact that these wounds were moderately exudative. The pre-hydration of hydrogel foams may have limited their absorbency, thus creating an overly moist wound environment that can have a negative impact on the surrounding skin. This was not specifically examined in our study, but further investigation into the healing outcome of GaM-loaded hydrogel foam with appropriate self-tuning moisture balance control may improve the ability of GaM-loaded hydrogels to have an even more positive impact on wound healing.

5. Conclusion

In this work, we investigated the antimicrobial activity of GaM against wound-specific MSSA and MRSA compared to gentamicin and vancomycin. In combination with the dose effects of these antimicrobial agents on hDFs, GaM was featured with a higher selectivity index than gentamicin and lower cytotoxicity than vancomycin. In addition, GaM demonstrated no adverse effect on hDF proliferation and collagen synthesis at a lower concentration. Based on these findings, GaM has shown promise as a new antimicrobial agent to treat chronic wounds with less risk of developing bacterial resistance. For controlled GaM release, an electrospraying toolbox was developed and utilized to fabricate GaM-loaded PLGA microspheres with tunable release profiles. We successfully incorporated GaM-loaded microspheres in previously developed porous hydrogel foam to make the GaM-loaded antimicrobial hydrogel foam. The microsphere size, GaM loading, and microsphere concentration modulated the GaM release profile to meet the requirement for sustained bacterial inhibition for the dressing application period. The *in vitro* evaluations of the GaM-loaded hydrogel foam showed no cytotoxicity and confirmed its antimicrobial activity. The *in vivo* study assessed the efficacy of this GaM-loaded hydrogel foam in a novel model of wound healing and demonstrated positive effects that were in line with our *in vitro* studies. Retaining the function of moisture balance control maintenance, this antimicrobial hydrogel foam dressing inhibited bacterial infection. Further investigation may focus on a more comprehensive evaluation of the bacterial resistance to GaM and *in vivo* efficacy of this antimicrobial dressing. Still, this antimicrobial hydrogel foam dressing has been confirmed to be a potent candidate to control bacterial infection and accelerate the closure of infected chronic wounds, preventing cellulitis or sepsis.

Ethics approval and consent to participate

The authors declare that there are no human subjects used in this research paper. The protocol for an equine distal limb wound model applied in this study was approved by the University's Institutional Animal Care and Use Committee (protocol A2022 05–003-Y2-A1).

CRediT authorship contribution statement

Ziyang Lan: Writing – original draft, Visualization, Methodology, Investigation, Formal analysis, Data curation, Conceptualization. **Leopold Guo:** Software, Methodology, Data curation. **Alan Fletcher:** Methodology, Data curation. **Nicolai Ang:** Software, Data curation. **Canaan Whitfield-Cargile:** Writing – original draft, Resources, Methodology, Formal analysis, Data curation, Conceptualization. **Laura Bryan:** Formal analysis, Data curation. **Shannara Welch:** Formal analysis, Data curation. **Lauren Richardson:** Formal analysis, Data curation. **Elizabeth Cosgriff-Hernandez:** Writing – review & editing, Supervision, Project administration, Funding acquisition, Conceptualization.

Declaration of competing interest

The authors declare that they have no known competing financial interests or personal relationships that could have appeared to influence the work reported in this paper.

Acknowledgment

This work was supported by National Institutes of Health (Grant No. R21 AR076107).

Appendix A. Supplementary data

Supplementary data to this article can be found online at https://doi.org/10.1016/j.bioactmat.2024.08.044.

References

[1] S. Kapp, N. Santamaria, The financial and quality-of-life cost to patients living with a chronic wound in the community, Int. Wound J. 14 (6) (2017) 1108–1119.
[2] S. Gupta, S. Sagar, S. Tripathi, T. Kisaka, G. Maheshwari, Chronic wounds -magnitude, socioeconomic burden and consequences, Wounds Asia 4 (1) (2021. 2021 Mar 15) 8–14.
[3] R.G. Frykberg, J. Banks, Challenges in the treatment of chronic wounds, Adv. Wound Care 4 (9) (2015 Sep 1) 560–582.
[4] L. Jiang, S.C.J. Loo, Intelligent nanoparticle-based dressings for bacterial wound infections, ACS Appl. Bio Mater. 4 (5) (2021 May 17) 3849–3862.
[5] Brem H, Tarnovskaya A, Baskin-Bey E, Clinic M. Healing of Elderly Patients with Diabetic Foot Ulcers, Venous Stasis Ulcers, and Pressure Ulcers. General Surgery.
[6] M. Falcone, B. De Angelis, F. Pea, A. Scalise, S. Stefani, R. Tasinato, et al., Challenges in the management of chronic wound infections, J. Global Antimicrobial Resista. 26 (2021 Sep 1) 140–147.
[7] A. Kingsley, The wound infection continuum and its application to clinical practice, Ostomy/Wound Manag. 49 (7A Suppl) (2003) 1–7.
[8] D. Leaper, O. Assadian, C e Edmiston, Approach to chronic wound infections, Br. J. Dermatol. 173 (2) (2015) 351–358.
[9] K. Gjødsbøl, J.J. Christensen, T. Karlsmark, B. Jørgensen, B.M. Klein, K.A. Krogfelt, Multiple bacterial species reside in chronic wounds: a longitudinal study, Int. Wound J. 3 (3) (2006) 225–231.
[10] M. Burmølle, T.R. Thomsen, M. Fazli, I. Dige, L. Christensen, P. Homøe, et al., Biofilms in chronic infections – a matter of opportunity – monospecies biofilms in multispecies infections, FEMS Immunol. Med. Microbiol. 59 (3) (2010 Aug 1) 324–336.
[11] T. Høgsberg, T. Bjarnsholt, J.S. Thomsen, K. Kirketerp-Møller, Success rate of split-thickness skin grafting of chronic venous leg ulcers depends on the presence of Pseudomonas aeruginosa: a retrospective study, PLoS One 6 (5) (2011 May 31) e20492.
[12] L. Deng, C. Du, P. Song, T. Chen, S. Rui, D.G. Armstrong, et al., The role of oxidative stress and antioxidants in diabetic wound healing, Oxid. Med. Cell. Longev. 2021 (2021 Feb 8) e8852759.
[13] A. Parnham, C. Bousfield, The influence of matrix metalloproteases and biofilm on chronic wound healing: a discussion, Br. J. Community Nurs. 23 (Sup3) (2018 Mar 2) S22–S29.

[14] F. Song, H. Koo, D. Ren, Effects of material properties on bacterial adhesion and biofilm formation, J. Dent. Res. 94 (8) (2015 Aug) 1027–1034.
[15] G.P. Marshall, J. Cserny, C.W. Wang, B. Looney, A.L. Posgai, R. Bacher, et al., Biomaterials-based nanoparticles conjugated to regulatory T cells provide a modular system for localized delivery of pharmacotherapeutic agents, J. Biomed. Mater. Res. 111 (2) (2023) 185–197.
[16] D. Kuczyńska-Wiśnik, E. Matuszewska, B. Furmanek-Blaszk, D. Leszczyńska, A. Grudowska, P. Szczepaniak, et al., Antibiotics promoting oxidative stress inhibit formation of Escherichia coli biofilm via indole signalling, Res. Microbiol. 161 (10) (2010 Dec) 847–853.
[17] S. Huang, S. Xu, Y. Hu, X. Zhao, L. Chang, Z. Chen, et al., Preparation of NIR-responsive, ROS-generating and antibacterial black phosphorus quantum dots for promoting the MRSA-infected wound healing in diabetic rats, Acta Biomater. 137 (2022 Jan 1) 199–217.
[18] F. Baquero, J.L. Martínez, R. Cantón, Antibiotics and antibiotic resistance in water environments, Curr. Opin. Biotechnol. 19 (3) (2008 Jun 1) 260–265.
[19] S. Sengupta, M. Chattopadhyay, H.P. Grossart, The multifaceted roles of antibiotics and antibiotic resistance in nature, Front. Microbiol. 4 (2013) 47.
[20] M. Zubair, A. Malik, J. Ahmad, Clinico-microbiological study and antimicrobial drug resistance profile of diabetic foot infections in North India, Foot 21 (1) (2011 Mar 1) 6–14.
[21] J.P. Morgan, R.H. Haug, J.W. Kosman, Antimicrobial skin preparations for the maxillofacial region, J. Oral Maxillofac. Surg. 54 (1) (1996 Jan 1) 89–94.
[22] R.A. Cooper, Iodine revisited, Int. Wound J. 4 (2) (2007) 124–137.
[23] M.S. Opstrup, G.B.E. Jemec, L.H. Garvey, Chlorhexidine allergy: on the rise and often overlooked, Curr. Allergy Asthma Rep. 19 (5) (2019 Mar 14) 23.
[24] J.M. Yabes, B.K. White, C.K. Murray, C.J. Sanchez, K. Mende, M.L. Beckius, et al., In Vitro activity of Manuka Honey and polyhexamethylene biguanide on filamentous fungi and toxicity to human cell lines, Med. Mycol. 55 (3) (2017 Apr 1) 334–343.
[25] S.F. Lo, M. Hayter, C.J. Chang, W.Y. Hu, L.L. Lee, A systematic review of silver-releasing dressings in the management of infected chronic wounds, J. Clin. Nurs. 17 (15) (2008) 1973–1985.
[26] S.L. Percival, P.G. Bowler, D. Russell, Bacterial resistance to silver in wound care, J. Hosp. Infect. 60 (1) (2005 May 1) 1–7.
[27] L.W. Toy, L. Macera, Evidence-based review of silver dressing use on chronic wounds, J. Am. Acad. Nurse Pract. 23 (4) (2011) 183–192.
[28] R. Warriner, R. Burrell, Infection and the chronic wound: a focus on silver, Adv. Skin Wound Care 18 (8) (2005 Oct) 2.
[29] A. Bahar, D. Ren, Antimicrobial peptides, Pharmaceuticals 6 (12) (2013 Nov 28) 1543–1575.
[30] R.J. Martens, K. Mealey, N.D. Cohen, J.R. Harrington, M.K. Chaffin, R.J. Taylor, et al., Pharmacokinetics of gallium maltolate after intragastric administration in neonatal foals, Am. J. Vet. Res. 68 (10) (2007 Oct 1) 1041–1044.
[31] S. Cereceres, Z. Lan, L. Bryan, M. Whitely, T. Wilems, H. Greer, et al., Bactericidal activity of 3D-printed hydrogel dressing loaded with gallium maltolate, APL Bioeng. 3 (2) (2019 Jun) 026102.
[32] Y.I. Jeong, D.G. Kim, D.H. Seo, M.K. Jang, J.W. Nah, Multiparticulation of ciprofloxacin HCl-encapsulated chitosan microspheres using poly(dl-lactide-co-glycolide), J. Ind. Eng. Chem. 14 (6) (2008 Nov 1) 747–751.
[33] K.G. Janoria, A.K. Mitra, Effect of lactide/glycolide ratio on the in vitro release of ganciclovir and its lipophilic prodrug (GCV-monobutyrate) from PLGA microspheres, Int. J. Pharm. 338 (1) (2007 Jun 29) 133–141.
[34] I. Amjadi, M. Rabiee, M.S. Hosseini, M. Mozafari, Synthesis and characterization of doxorubicin-loaded poly(lactide-co-glycolide) nanoparticles as a sustained-release anticancer drug delivery system, Appl. Biochem. Biotechnol. 168 (6) (2012 Nov 1) 1434–1447.
[35] Y. Su, B. Zhang, R. Sun, W. Liu, Q. Zhu, X. Zhang, et al., PLGA-based biodegradable microspheres in drug delivery: recent advances in research and application, Drug Deliv. 28 (1) (2021 Jan 1) 1397–1418.
[36] N. Bock, T.R. Dargaville, M.A. Woodruff, Electrospraying of polymers with therapeutic molecules: state of the art, Prog. Polym. Sci. 37 (11) (2012 Nov) 1510–1551.
[37] Z. Lan, R. Kar, M. Chwatko, E. Shoga, E. Cosgriff-Hernandez, High porosity PEG-based hydrogel foams with self-tuning moisture balance as chronic wound dressings, J. Biomed. Mater. Res. 111 (4) (2023) 465–477.
[38] T.W. Buie, M. Whitely, J. McCune, Z. Lan, A. Jose, A. Balakrishnan, et al., Comparative efficacy of resorbable fiber wraps loaded with gentamicin sulfate or gallium maltolate in the treatment of osteomyelitis, J. Biomed. Mater. Res. 109 (11) (2021 Nov) 2255–2268.
[39] Methods for Dilution Antimicrobial Susceptibility Tests for Bacteria that Grow Aerobically; Approved Standard. 950 West Valley Road, Suite 2500, Wayne, Pennsylvania 19087, Clinical and Laboratory Standards Institute, USA, 2012.
[40] K.A. Wegner, A. Keikhosravi, K.W. Eliceiri, C.M. Vezina, Fluorescence of picrosirius red multiplexed with immunohistochemistry for the quantitative assessment of collagen in tissue sections, J. Histochem. Cytochem. 65 (8) (2017 Aug) 479–490.
[41] M.S. Hahn, L.J. Taite, J.J. Moon, M.C. Rowland, K.A. Ruffino, J.L. West, Photolithographic patterning of polyethylene glycol hydrogels, Biomaterials 27 (12) (2006 Apr 1) 2519–2524.
[42] S.P. Lawless, N.D. Cohen, S.D. Lawhon, A.M. Chamoun-Emanuelli, J. Wu, A. Rivera-Vélez, et al., Effect of gallium maltolate on a model of chronic, infected equine distal limb wounds, PLoS One 15 (6) (2020 Jun 19) e0235006.
[43] A.K. Brock, A.M. Chamoun-Emanuelli, E.A. Howard, K.D. Huntzinger, S. D. Lawhon, L.K. Bryan, et al., Wound swabs versus biopsies to detect methicillin resistant *staphylococcus aureus* in experimental equine wounds, Vet. Surg. 51 (8) (2022 Nov) 1196–1205.
[44] R.H.T. Nijhuis, N.M. Van Maarseveen, E.J. Van Hannen, A.A. Van Zwet, E. M. Mascini, A rapid and high-throughput screening approach for methicillin-resistant staphylococcus aureus based on the combination of two different real-time PCR assays, in: G.V. Doern (Ed.), J. Clin. Microbiol. 52 (8) (2014 Aug) 2861–2867.
[45] É. Lepault, C. Céleste, M. Doré, D. Martineau, C.L. Theoret, Comparative study on microvascular occlusion and apoptosis in body and limb wounds in the horse, Wound Repair Regen. 13 (5) (2005) 520–529.
[46] S.J. Landis, Chronic wound infection and antimicrobial use, Adv. Skin Wound Care 21 (11) (2008 Nov) 531.
[47] G. Zhao, M.L. Usui, S.I. Lippman, G.A. James, P.S. Stewart, P. Fleckman, et al., Biofilms and inflammation in chronic wounds, Adv. Wound Care 2 (7) (2013 Sep) 389–399.
[48] D. Metcalf, P. Bowler, Biofilm delays wound healing: a review of the evidence, Burn Trauma 1 (1) (2013) 5.
[49] G. Zhao, M.L. Usui, R.A. Underwood, P.K. Singh, G.A. James, P.S. Stewart, et al., Time course study of delayed wound healing in a biofilm-challenged diabetic mouse model: delayed healing in biofilm-colonized db/db mouse wounds, Wound Repair Regen. 20 (3) (2012 May) 342–352.
[50] R.A. Cooper, T. Bjarnsholt, M. Alhede, Biofilms in wounds: a review of present knowledge, J. Wound Care 23 (11) (2014 Nov 2) 570–582.
[51] S. Veerachamy, T. Yarlagadda, G. Manivasagam, P.K. Yarlagadda, Bacterial adherence and biofilm formation on medical implants: a review, Proc. Inst. Mech. Eng. H 228 (10) (2014 Oct) 1083–1099.
[52] B.H. Bradley, M. Cunningham, Biofilms in chronic wounds and the potential role of negative pressure wound therapy: an integrative review, J. Wound, Ostomy Cont. Nurs. 40 (2) (2013 Apr) 143.
[53] J.G. Powers, C. Higham, K. Broussard, T.J. Phillips, Wound healing and treating wounds: chronic wound care and management, J. Am. Acad. Dermatol. 74 (4) (2016 Apr 1) 607–625.
[54] L. Atkin, Understanding methods of wound debridement, Br. J. Nurs. 23 (sup12) (2014 Jun) S10–S15.
[55] B.M. Madhok, K. Vowden, P. Vowden, New techniques for wound debridement: new techniques for wound debridement, Int. Wound J. 10 (3) (2013 Jun) 247–251.
[56] S. Steingrimsson, M. Gottfredsson, I. Gudmundsdottir, J. Sjogren, T. Gudbjartsson, Negative-pressure wound therapy for deep sternal wound infections reduces the rate of surgical interventions for early re-infections, Interact. Cardiovasc. Thorac. Surg. 15 (3) (2012 Sep 1) 406–410.
[57] A. Saadi, J.Y. Perentes, M. Gonzalez, A.C. Tempia, Y. Wang, N. Demartines, et al., Vacuum-assisted closure device: a useful tool in the management of severe intrathoracic infections, Ann. Thorac. Surg. 91 (5) (2011 May) 1582–1589.
[58] A. Braakenburg, M.C. Obdeijn, R. Feitz, I.A.L.M. Van Rooij, A.J. Van Griethuysen, J.H.G. Klinkenbijl, The clinical efficacy and cost effectiveness of the vacuum-assisted closure technique in the management of acute and chronic wounds: a randomized controlled trial, Plast. Reconstr. Surg. 118 (2) (2006 Aug) 390–397.
[59] A.S.P. Patmo, P. Krijnen, W.E. Tuinebreijer, R.S. Breederveld, The effect of vacuum-assisted closure on the bacterial load and type of bacteria: a systematic review, Adv. Wound Care 3 (5) (2014 May) 383–389.
[60] H.C. Neu, The crisis in antibiotic resistance, Science 257 (5073) (1992 Aug 21) 1064–1073.
[61] O. Sarheed, A. Ahmed, D. Shouqair, J. Boateng, Antimicrobial dressings for improving wound healing, in: V.A. Alexandrescu (Ed.), Wound Healing - New Insights into Ancient Challenges, InTech, 2016 October, pp. 373–398.
[62] L.R. Bernstein, T. Tanner, C. Godfrey, B. Noll, Chemistry and pharmacokinetics of gallium maltolate, a compound with high oral gallium bioavailability, Met. Base. Drugs 7 (1) (2000 Jan 1) 33–47.
[63] C.R. Chitambar, D.P. Purpi, J. Woodliff, M. Yang, J.P. Wereley, Development of gallium compounds for treatment of lymphoma: gallium maltolate, a novel hydroxypyrone gallium compound, induces apoptosis and circumvents lymphoma cell resistance to gallium nitrate, J. Pharmacol. Exp. Therapeut. 322 (3) (2007 Sep 1) 1228–1236.
[64] M.S. Chua, L.R. Bernstein, R. Li, S.K.S. So, Gallium maltolate is a promising chemotherapeutic agent for the treatment of hepatocellular carcinoma, Anticancer Res. 26 (3A) (2006 May 1) 1739–1743.
[65] Y. Kaneko, M. Thoendel, O. Olakanmi, B.E. Britigan, P.K. Singh, The transition metal gallium disrupts *Pseudomonas aeruginosa* iron metabolism and has antimicrobial and antibiofilm activity, J. Clin. Invest. 117 (4) (2007 Apr 2) 877–888.
[66] K. DeLeon, F. Balldin, C. Watters, A. Hamood, J. Griswold, S. Sreedharan, et al., Gallium maltolate treatment eradicates Pseudomonas aeruginosa infection in thermally injured mice, Antimicrob. Agents Chemother. 53 (4) (2009 Apr) 1331–1337.
[67] C.E. Arnold, A. Bordin, S.D. Lawhon, M.C. Libal, L.R. Bernstein, N.D. Cohen, Antimicrobial activity of gallium maltolate against Staphylococcus aureus and methicillin-resistant S. aureus and Staphylococcus pseudintermedius: an in vitro study, Vet. Microbiol. 155 (2) (2012 Mar 23) 389–394.
[68] B. Khameneh, M. Iranshahy, M. Ghandadi, D. Ghoochi Atashbeyk, B.S. Fazly Bazzaz, M. Iranshahi, Investigation of the antibacterial activity and efflux pump inhibitory effect of co-loaded piperine and gentamicin nanoliposomes in methicillin-resistant Staphylococcus aureus, Drug Dev. Ind. Pharm. 41 (6) (2015 Jun 3) 989–994.
[69] R. Mao, D. Teng, X. Wang, D. Xi, Y. Zhang, X. Hu, et al., Design, expression, and characterization of a novel targeted plectasin against methicillin-resistant Staphylococcus aureus, Appl. Microbiol. Biotechnol. 97 (9) (2013 May 1) 3991–4002.

[70] V.H. Tam, S. Kabbara, G. Vo, A.N. Schilling, E.A. Coyle, Comparative pharmacodynamics of gentamicin against Staphylococcus aureus and Pseudomonas aeruginosa, Antimicrob. Agents Chemother. 50 (8) (2006 Aug) 2626–2631.
[71] Y. Xia, X. Wang, X. Wen, K. Ding, J. Zhou, Y. Yang, et al., Overall functional gene diversity of microbial communities in three full-scale activated sludge bioreactors, Appl. Microbiol. Biotechnol. (2014 May 10) 98.
[72] X. Wu, T.W. Wang, G.M. Lessmann, J. Saleh, X. Liu, C.R. Chitambar, et al., Gallium maltolate inhibits human cutaneous T-cell lymphoma tumor development in mice, J. Invest. Dermatol. 135 (3) (2015 Mar) 877–884.
[73] M.M. Al-Gizawiy, R.T. Wujek, H.S. Alhajala, J.M. Cobb, M.A. Prah, N.B. Doan, et al., Potent in vivo efficacy of oral gallium maltolate in treatment-resistant glioblastoma, Front. Oncol. 13 (2024 Jan 15) 1278157.
[74] F. Strodtbeck, Physiology of wound healing, N.born Infant Nurs. Rev. 1 (1) (2001) 43–52.
[75] S. Enoch, D.J. Leaper, Basic science of wound healing, Surgery 26 (2) (2008) 31–37.
[76] G. Hosgood, Stages of wound healing and their clinical relevance, Veterinary Clinics: Small Animal Practice 36 (4) (2006) 667–685.
[77] S.S. Mathew-Steiner, S. Roy, C.K. Sen, Collagen in wound healing, Bioengineering 8 (5) (2021 May) 63.
[78] D.P. Kelsen, N. Alcock, S. Yeh, J. Brown, C. Young, Pharmacokinetics of gallium nitrate in man, Cancer 46 (9) (1980) 2009–2013.
[79] L.R. Bernstein, T. Tanner, C. Godfrey, B. Noll, Chemistry and pharmacokinetics of gallium maltolate, a compound with high oral gallium bioavailability, Met-based Drugs. 7 (1) (2000 Jan) 33–47.
[80] S. Zhang, C. Campagne, F. Salaün, Preparation of electrosprayed poly (caprolactone) microparticles based on green solvents and related investigations on the effects of solution properties as well as operating parameters, Coatings 9 (2) (2019 Jan 30) 84.
[81] L.C. Chen, K. Nishidate, Y. Saito, K. Mori, D. Asakawa, S. Takeda, et al., Characteristics of probe electrospray generated from a solid needle, J. Phys. Chem. B 112 (35) (2008 Sep 4) 11164–11170.
[82] D. Zahn, A. Weidner, Z. Nosrati, L. Wöckel, J. Dellith, R. Müller, et al., Temperature controlled camptothecin release from biodegradable magnetic PLGA microspheres, J. Magn. Magn Mater. 469 (2019 Jan 1) 698–703.
[83] G. Kang, Y. Cao, H. Zhao, Q. Yuan, Preparation and characterization of crosslinked poly(ethylene glycol) diacrylate membranes with excellent antifouling and solvent-resistant properties, J. Membr. Sci. 318 (1) (2008 Jun 20) 227–232.
[84] K. Ubukata, R. Nonoguchi, M. Matsuhashi, M. Konno, Expression and inducibility in Staphylococcus aureus of the mecA gene, which encodes a methicillin-resistant S. aureus-specific penicillin-binding protein, J. Bacteriol. 171 (5) (1989 May) 2882–2885.
[85] L.G.M. Bode, P. van Wunnik, N. Vaessen, P.H.M. Savelkoul, L.C. Smeets, Rapid detection of methicillin-resistant Staphylococcus aureus in screening samples by relative quantification between the mecA gene and the SA442 gene, J. Microbiol. Methods 89 (2) (2012 May 1) 129–132.